JGR Biogeosciences

RESEARCH ARTICLE
10.1029/2023JG007532

A Tale of Two Catchments: Causality Analysis and Isotope Systematics Reveal Mountainous Watershed Traits That Regulate the Retention and Release of Nitrogen

N. J. Bouskill[1], M. Newcomer[1], R. W. H. Carroll[2,3], C. Beutler[3], M. Bill[1], W. S. Brown[3], M. Conrad[1], W. S. Dong[1], N. Falco[1], T. Maavara[4], A. Newman[3], P. O. Sorensen[1], T. K. Tokunaga[1], J. Wan[1], H. Wainwright[1], Q. Zhu[1], E. L. Brodie[1], and K. H. Williams[1,3]

[1]Earth and Environmental Sciences Area, Lawrence Berkeley National Laboratory, Berkeley, CA, USA, [2]Desert Research Institute, Reno, NV, USA, [3]Rocky Mountain Biological Laboratory, Gothic, CO, USA, [4]School of Geography, University of Leeds, Leeds, UK

Abstract Mountainous watersheds are characterized by variability in functional traits, including vegetation, topography, geology, and geomorphology, which determine nitrogen (N) retention, and release. Coal Creek and East River are two contrasting catchments within the Upper Colorado River Basin that differ markedly in total nitrate (NO_3^-) export. The East River has a diverse vegetation cover, and sinuous floodplains, and is underlain by N-rich marine shale. At 0.21 ± 0.14 kg ha^{-1} yr^{-1}, the East River exports ~3.5 times more NO_3^- relative to the conifer-dominated Coal Creek (0.06 ± 0.02 kg ha^{-1} yr^{-1}). While this can partly be explained by the larger size of the East River, the distinct watershed traits of these two catchments imply different mechanisms controlling the aggregate N-export signal. A causality analysis shows physical and biogenic processes were critical in determining NO_3^- export from the East River catchment. Stable isotope ratios of NO_3^- ($\delta^{15}N_{NO3}$ and $\delta^{18}O_{NO3}$) show the East River catchment is a strong hotspot for biogeochemical processing of NO_3^- at the hillslope soil-saprolite. By contrast, the conifer-dominated Coal Creek retained nearly all atmospherically deposited NO_3^-, and its export was controlled by catchment hydrological traits (i.e., snowmelt periods and water table depth). The conservative N-cycle within Coal Creek is likely due to the abundance of conifer trees, and smaller riparian regions, retaining more NO_3^- overall and reduced processing prior to export. This study highlights the value of integrating isotope systematics to link watershed functional traits to mechanisms of watershed element retention and release.

Plain Language Summary The role different functional traits play in the retention and release of nitrogen remains uncertain. Here we describe how two neighboring catchments in the Upper Colorado River Basin, characterized by contrasting vegetation, geology, and geomorphology, cycle and export nitrogen. The East River catchment, which is underlain by nitrogen-rich shale, and has a diverse vegetation cover, releases over three times as much nitrate (NO_3^-) than the conifer-dominated Coal Creek, which is underlain by granitic rock. However, a suite of analyses show that the distinct watershed traits of these two catchments lead to diverse pathways of nitrogen cycling. Biogenic processes, critical to determining NO_3^- export in East River, impart strong biogeochemical processing prior to export. By contrast, Coal Creek retains almost all of the atmospherically deposited NO_3^-, likely due to uptake by conifers, and a small riparian region. This study highlights the use of nitrate isotope systematics to parse different mechanisms leading to NO_3^- export.

Key Points:

- Comparing and contrasting neighboring catchments identifies watershed traits regulating the cycling, retention and release of nitrogen
- Conifer forest-dominated catchments show a conservative nitrogen cycling, retaining ~97% of atmospherically dominated nitrate
- By contrast, meadow-dominated catchments underlain Mancos shale are biogeochemical hotspots for N-cycling, and export higher nitrate loads

Supporting Information:

Supporting Information may be found in the online version of this article.

Correspondence to:

N. J. Bouskill,
njbouskill@lbl.gov

Citation:

Bouskill, N. J., Newcomer, M., Carroll, R. W. H., Beutler, C., Bill, M., Brown, W. S., et al. (2024). A Tale of two catchments: Causality analysis and isotope systematics reveal mountainous watershed traits that regulate the retention and release of nitrogen. *Journal of Geophysical Research: Biogeosciences*, *129*, e2023JG007532. https://doi.org/10.1029/2023JG007532

Received 27 APR 2023
Accepted 27 FEB 2024

Author Contributions:

Conceptualization: N. J. Bouskill, M. Conrad, T. Maavara, K. H. Williams
Data curation: N. J. Bouskill, R. W. H. Carroll, W. S. Dong
Formal analysis: N. J. Bouskill, R. W. H. Carroll, C. Beutler, M. Bill, W. S. Brown, M. Conrad, W. S. Dong, A. Newman, P. O. Sorensen, T. K. Tokunaga, J. Wan, H. Wainwright, Q. Zhu, E. L. Brodie, K. H. Williams
Funding acquisition: N. J. Bouskill, E. L. Brodie, K. H. Williams
Investigation: N. J. Bouskill

1. Introduction

Strong variability in stream water chemistry between neighboring headwater catchments can provide insight into how watershed traits (e.g., gradients in bedrock, topography, aspect, and land cover) interact to modulate retention and release of critical elements and thus influence downstream water quality (Alexander et al., 2007; McDonnell et al., 2007). Nitrogen, which often limits ecosystem processes within mountainous watersheds (Campbell et al., 2002; Kou et al., 2020; Thébault et al., 2014), enters through several pathways, including by atmospheric deposition of inorganic and organic nitrogen (Clark et al., 2021), bedrock weathering (Holloway et al., 1998; Houlton et al., 2018; Wan et al., 2021), and nitrogen fixation (Moyes et al., 2016). Retention within the ecosystem occurs primarily through plant acquisition, microbial immobilization (Goodale, 2017; Zogg et al., 2000), and groundwater storage (Ascott et al., 2017). Loss of nitrogen occurs through denitrification within

Methodology: N. J. Bouskill, R. W. H. Carroll, Q. Zhu
Project administration: N. J. Bouskill, E. L. Brodie, K. H. Williams
Resources: N. J. Bouskill, C. Beutler, M. Conrad, N. Falco, P. O. Sorensen, T. K. Tokunaga, J. Wan, K. H. Williams
Software: N. J. Bouskill, H. Wainwright, Q. Zhu
Supervision: K. H. Williams
Validation: N. J. Bouskill, N. Falco, T. Maavara
Visualization: N. J. Bouskill
Writing – original draft: N. J. Bouskill
Writing – review & editing: N. J. Bouskill, R. W. H. Carroll, C. Beutler, M. Bill, W. S. Brown, M. Conrad, W. S. Dong, N. Falco, T. Maavara, A. Newman, P. O. Sorensen, T. K. Tokunaga, J. Wan, Q. Zhu, E. L. Brodie, K. H. Williams

variably saturated regions of the watershed (e.g., within floodplains, Bouskill et al., 2019; Gomez-Velez et al., 2015), the erosional deposition of particulate nitrogen (Berhe & Torn, 2017), or lateral flow of dissolved species to streams and rivers (Peterson, 2001; Rose et al., 2015).

The balance between the retention and release of nitrogen in headwater catchments is strongly coupled to the hydrological cycle (Maavara et al., 2021; Schimel et al., 1997; Zhu et al., 2018). The transit times of different solutes through the terrestrial biosphere are dictated by the contact time between water and reactive surfaces including microorganisms (Lansdown et al., 2015; Li et al., 2021; Pinay et al., 2015). The resultant stream water chemistry is derived from distinct water sources that reflect this transit time, and the magnitude of biogeochemical cycling of nitrogen along the various flow paths to the river. Depending on the time of year within snowmelt-dominated systems, the chemical signatures might reflect nitrogen derived from flow paths across distinct hillslope depths (Zhi et al., 2019, 2020), whereby shallow soils dominate solute flux to the river as the water table rises toward the surface during snowmelt (Zhi et al., 2019). Similarly, under baseflow conditions stream water chemistry reflects deeper groundwater-dominated sources.

The movement of water and nitrogen through the subsurface of mountainous catchments is also further modified through interactions with vegetation. Plant-nitrogen assimilation predominantly takes place from shallow soil layers, aided by the turnover of microbial biomass built-up under snowpack (Sorensen et al., 2020). Mycorrhizal-symbionts further regulate nutrient transfer from soils to plants (Hobbie & Högberg, 2012), and the relationship between plants and different mycorrhizal fungi shapes the nitrogen sources that can be accessed (Phillips et al., 2013; Ward et al., 2022). Moreover, the flux of nitrogen entering catchments is also dependent on litter decomposition as a function of litter quality (e.g., carbon: nitrogen ratios), which is related to species demographics and is a critical pathway of the nitrogen cycle in high-altitude soils (Maavara et al., 2021).

This study details how nitrogen is cycled and exported as a function of headwater catchment traits. We compare and contrast the nitrogen cycles of two catchments, Coal Creek and the main stem East River, within the wider East River watershed in the Upper Colorado River Basin, United States. These catchments differ in their underlying trait distribution, notably geology, dominant vegetation, geomorphology, and aspect (Hubbard et al., 2018). Herein we examine whether the contrasting biotic and abiotic traits that distinguish Coal Creek and the East River are apparent through divergent signals in nitrogen export.

To evaluate the different sources and behavior of riverine solutes from Coal Creek and East River catchments we initially analyzed the concentration-discharge (cQ) relationships of biogenic and geogenic solutes over a 5-year period. cQ relationships have been widely used to determine how catchments store and release water and solutes (Godsey et al., 2009; Knapp et al., 2020; Musolff et al., 2015; Thompson et al., 2011), and to partition between geogenic and biogenic sources as a function of the hydrograph (Zhi et al., 2019). This method uses a power law relationship to determine whether the behavior of a solute is chemostatic (i.e., unchanging concentration with increasing discharge), or chemodynamic (i.e., either increasing or decreasing with increasing discharge). However, because the cQ relationship can be insensitive to high variability in concentration data, we complemented this characterization by calculating the ratio between the coefficient of variation (CV) of NO_3^- concentration (CV_c) and discharge (CV_q). The CV_c/CV_q metric provides additional evidence for the various sources of solute mobilization by determining whether the underlying relationship in solute export is driven by variability in discharge or not (Basu et al., 2011; Knapp et al., 2022).

The relationship between solute concentration and discharge provides important information on their origin and mobility across different parts of the hydrograph. However, given the array of processes regulating the retention and release of NO_3^- from catchments (Bouskill et al., 2019; Clark et al., 2021; Wan et al., 2021) categorically relating NO_3^- export to the set of different functional traits within each catchment requires further analysis. Here, we employ a transfer entropy analysis (Ruddell & Kumar, 2009) that statistically relates the relative strength, directionality, and significance of different time series (e.g., variables related to biogenic or geogenic proxies) within a network of interacting and interdependent parameters. This approach robustly relates the export of NO_3^- from each paired catchment to distinct pathways, including snowmelt driven export of soil-derived NO_3^- relative to geogenic release of NO_3^-.

Finally, identifying the atmospheric and terrestrial sources and sinks that contribute to the aggregate NO_3^- export signal requires measurements of the stable isotopes of nitrate ($\delta^{15}N_{NO3}$ and $\delta^{18}O_{NO3}$) from both soil porewater, as well as Coal Creek and East River. The isotopic signature of nitrate represents the aggregated contribution of

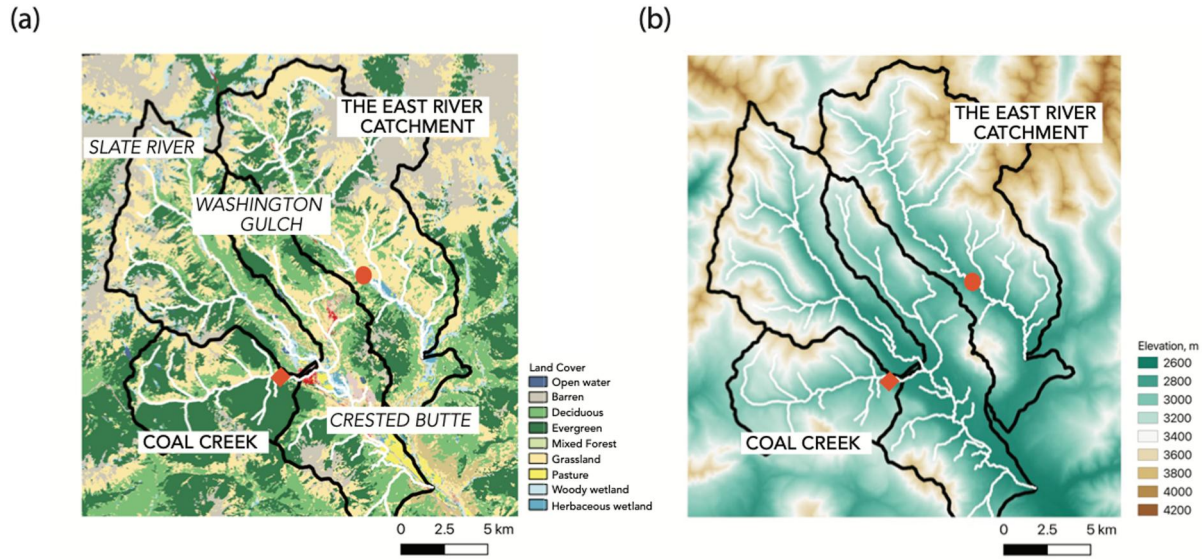

Figure 1. The East River watershed depicting (a) land cover and (b) elevation. On each panel the different catchments are demarcated by a black outline. With the Coal Creek catchment the river sampling point is denoted by the orange diamond, while the orange circle in the East Tiver catchment indicates the river sampling point, and the adjacent borehole transect for terrestrial porewater collection.

different sources and reflects both the strength of retention and the magnitude of biogeochemical cycling along different flow paths toward the river (Granger & Wankel, 2016). $\delta^{15}N_{NO3}$ and $\delta^{18}O_{NO3}$ can identify periods of high nitrate reduction through the monotonic enrichment in isotopic fractionation (Wexler et al., 2014), indicating prolonged transit times through the ecosystem. Moreover, the direct contribution of atmospheric nitrate to riverine export can be identified through high $\delta^{18}O_{NO3}$ (~60–80‰) imparted during the atmospheric formation of nitrate (Michalski et al., 2012), and this isotopic signal can be used to quantify retention of atmospheric nitrate by vegetation and microbes.

We use these complementary data sets to address two main objectives: Our first objective seeks to compare and contrast nitrate export within two neighboring catchments differing in functional trait distribution while sharing the same climate and nitrogen deposition patterns. A second objective focuses on the East River catchment and leverages existing borehole infrastructure, not available in Coal Creek, to relate riverine nitrate export to nitrogen cycling across a hillslope-toeslope-floodplain continuum adjoining the river.

2. Materials and Methods

2.1. Study Site

The East River watershed (38° 57.5' N, 106° 59.3' W) is a representative headwater system in the West Elk Mountains near the towns of Crested Butte and Gothic, Colorado (USA) within the Upper Colorado Basin (Hubbard et al., 2018). The East River is a major tributary to the Gunnison River, which accounts for almost half of the Colorado River's discharge at the border with Utah. The East River watershed is approximately 300 km^2 (Figure 1), and encompasses the main stem East River (including the current study site East River at Pumphouse), Slate River, Washington Gulch, and Coal Creek (Figure 1a). The East River watershed is a large watershed of the hydrologic unit code 10 (USGS: HUC10 East River Watershed: #1402000102)), characterized by the intersection of two HUC12 catchments. The East River at Pumphouse is made up of the smaller HUC12 catchments (#140200010201 Upper East River) which drains to the HUC12 #140200010202 Brush Creek catchment where the Pumphouse is located. For clarity, the catchment, East River at Pumphouse, is hereafter referred to as ERP, to avoid confusion with the larger East River watershed. Coal Creek is a defined HUC12 catchment (#140200010204 Coal Creek) of the HUC10 East River Watershed (#1402000102).

The East River watershed has an average elevation of 3,266 m, and ranges from 2,750 to 4,000 m (Figure 1b). The area has a continental, subarctic climate, with a mean annual temperature of 0°C, and average minimum and

maximum temperatures of −9.2 and 9.8°C, respectively. Mean annual precipitation is ∼1,200 mm yr^{-1}, with the majority (>80%) falling as snow, and much of the rest falling during the monsoonal period in late summer and fall (Carroll et al., 2020). Snowfall and melt dominate the hydrological cycle, as is typical for mountainous systems in the Western United States (Li et al., 2017), and losses are partitioned between evapotranspiration and streamflow, which differ in their contributions based on several characteristics, including a higher ET flux with higher proportional tree cover (Sprenger et al., 2022). Runoff characteristics for both catchments are similar in terms of the timing of peak discharge in early June and the transition to baseflow in late September-early October, where groundwater represents a significant fraction of streamflow (Hubbard et al., 2018).

Atmospheric deposition of wet and dry forms of reactive nitrogen (nitrate and ammonium) for the East River watershed was extracted from the EPA CASTNET continuous monitoring system located at Gothic (https://www3.epa.gov/castnet/site_pages/GTH161.html), and from the broader national atmospheric deposition program (https://nadp.slh.wisc.edu/committees/tdep/). Annual nitrogen deposition averaged 2–3 kg-N ha^{-1} over a 17-year period (2000–2017). Historically, oxidized inorganic nitrogen was the dominant species contributing to the total atmospheric deposition, however, since 2011, deposition has been split between reduced and oxidized inorganic nitrogen (Figure S1 in Supporting Information S1), which is likely attributable to a lack of regulation on NH_4^+ emissions (Li et al., 2016). The contribution of anthropogenic nitrogen to total deposition in the different watersheds remains uncertain, yet, a recent quantification of phosphorus deposition in the East River watershed used lead isotopes ($^{206}Pb/^{207}Pb$ and $^{208}Pb/^{207}Pb$) to estimate that up to 59% (mean = 37%) of atmospheric dust derived from anthropogenic sources.

A recent analysis for the wider East River watershed separates these two catchments based on their comparative disparity in traits including catchment size, aspect, average slope, vegetation (including normal difference vegetation index), and geology (Wainwright et al., 2022). At 56 km^2, Coal Creek exhibits an east-west orientation, with north- and south-facing hillslope aspects, and an average slope of 16°. The characteristics of this catchment have been described previously (Zhi et al., 2020). The land cover is approximately 60% evergreen forests (e.g., mainly *Pinus contorta but also Abies spp*.) with 10% montane plants and shrubs (e.g., *Artemisia tridentata*), and 11% riparian shrubland (dominated by *Salix monticola*). Only 1% of land is barren. The underlying bedrock is dominated by sedimentary and igneous rock types (including areas of significant mineralization by pyritic ore minerals and associated historic mines). These primarily include sandstone (39%) and mudstone (15%) from the Late Cretaceous Mesa Verde formation and Neogene Ohio Creek and Wasatch formations (Manning et al., 2008; Uhlemann et al., 2022). Supplementing these sedimentary units are plutonic rocks (15%) dominated by granodiorite and quartz monzonite of Oligocene age.

By contrast, the 86 km^2 main stem of the ERP intensive study site is oriented in a northwest-southeast direction, with an average slope 23°. Land cover within the ERP is more heterogeneous than that of Coal Creek, with extensive regions of barren alpine and subalpine land, mixed forest, including ∼10% deciduous forest (*Populus tremuloides*), ∼21% coverage by coniferous trees (predominantly *Picea engelmannii, and Abies lasiocarpa*), and 27% intermixed shrub- and grassland meadows. The meadow regions show a mix of perennial bunchgrass (e.g., *Festuca arizonica*), forbs (e.g., *Potentilla gracilis, Veratrum californicum, Lupinus spp.*), and shrubs (*Artemisia tridentata*). Relative to Coal Creek, the East River shows considerable sinuosity, and has an extensive riparian floodplain system dominated by dwarf birch (*Betula grandulosa*) and mountain willow (*Salix spp.*). Plant communities are largely underlain by Cretaceous Mancos shale bedrock (Hubbard et al., 2018), which is absent in Coal Creek, with glacial till also underlying the North Eastern end of the catchment. Agricultural influence is limited to summer grazing of cattle within the ERP (herd size ∼ 500 individuals).

The suite of measurements made in this study, the start and end of the time series, the frequency of collection, and any necessary pre-processing, have been summarized in Table S1 in Supporting Information S1. Below we briefly describe the methods used in sample collection.

2.2. Borehole Installation

To link export patterns to nitrogen cycling within terrestrial ecosystems, we focused on a montane hillslope within the pumphouse intensive research site at the ERP. Five 10-m deep boreholes (0.14 m diameter) were drilled into bedrock along a 137 m-long hillslope-toeslope-floodplain transect. Specific drilling and instrumentation details of these boreholes have been published previously (Wan et al., 2021). Relevant to this study was the installation of porewater samplers, and moisture sensors from the O-horizon (at 0.28 and 1 m), through the weathered saprolite

(1.7 and 2.65 m), and into the bedrock at 4.7, 6.5, 6.7, and 8.2 m across the transect. Porewater samples were taken throughout the 2017–2019 period, inclusive of two anomalously high- and low-snowpack years.

2.3. Physicochemical Measurements

We collected measurements of streamflow and stream water chemistry across a 5-year, 9-month period covering 1 January 2016 through 30 September 2021. The analysis of the streamflow data has been described recently (Carroll et al., 2021). Stream- and porewater samples were collected for aqueous chemistry measurement using an automatic sampler (Teledyne ISCO 3700, NE, USA) attached to a peristaltic pump. Sampling frequency for stream water samples varied from once per week to three times per week depending on season. Snow was sampled synoptically by digging snow pits and sampling down through the depth of the pit. This depth was dependent on the snow year and varied between 0.4 and 1.6 m. Precipitation samples were also taken synoptically during the monsoonal period, which typically spans the late June to early September timeframe. Prior to anion or cation analysis, water samples were filtered through a 0.45 μm Millipore filter. The anion samples were collected into 2 ml polypropylene vials (with no headspace), and the cation samples were collected into high-density polyethylene vials, and acidified with ultra-pure concentrated nitric acid. Anions were measured through ion chromatography (Dionex ICS-2100, Thermo Scientific, USA), and aqueous cation concentration was determined using ICP-MS (Elan DRC II, Perkin Elmer, USA). Dissolved total nitrogen (DTN) was measured on all samples via thermal decomposition and chemiluminescence (Shimadzu TOC-VCSH with the attached TNM-1). Water samples for the determination of ammonium concentrations were taken as described above and measured on a Lachat (QuikChem 8,500 series 2 flow injection analysis system). Measurement of riverine properties (e.g., electrical chemistry, pH, dissolved oxygen, water temperature) were taken at the site of collection using a YSI data sonde.

2.4. Nitrate Isotope Measurements

The natural abundance of $\delta^{15}N_{NO3}$ and $\delta^{18}O_{NO3}$ in riverine and porewater, snow, and rainfall were measured using the denitrifier method as described previously (Bouskill et al., 2019), and in detail in the supplemental materials. Briefly, samples from either the river (40 ml) or lysimeters (50–100 ml) were filtered through a 0.2 μm Sterivex filter and placed on ice in the field. Samples were shipped overnight to Lawrence Berkeley National Laboratory and kept at −80°C until analysis. The isotope ratios of NO_3^- ($\delta^{15}N_{NO3}$ and $\delta^{18}O_{NO3}$), where δ (‰) = $(R_{NO3}/R_{std} - 1) * 1{,}000$, R indicates either $^{15}N/^{14}N$ or $^{18}O/^{16}O$, and 'std' refers to standard reference material, either N_2 in the air for $\delta^{15}N$ or Vienna standard mean ocean water (VSMOW) for $\delta^{18}O$, were measured via the denitrifier method (Casciotti & Buchwald, 2012; Sigman et al., 2001). Analysis of the isotopic data is described in detail in supplemental materials. Briefly, we used a simple mixing model to partition the isotopic signal of riverine NO_3^- between atmospheric and soil-derived sources. Furthermore, the change in $\delta^{15}N_{NO3}$ relative to that of $\delta^{18}O_{NO3}$ (i.e., $\Delta\delta^{18}O_{NO3}$: $\Delta\delta^{15}N_{NO3}$) was used in stream and porewater to determine whether a decline in NO_3^- concentrations could be due to source water mixing or due to fractionation mechanisms, as described previously (Granger & Wankel, 2016).

2.5. Analysis of Concentration-Discharge Relationships

Streamwater cQ relationships were initially described using a power law relationship ($c = aQ^b$) where a represents the intercept and the exponent, b, represents the slope of the cQ relationship (Musolff et al., 2015). The exponent provides information determining how the relationship between solute export changes with the hydrograph (Thompson et al., 2011). For example, $b = 0$ indicates a chemostatic relationship between discharge and solute concentration, a relationship characteristic of headwater catchments (Godsey et al., 2009). By contrast, positive or negative deviations from this relationship can represent solute mobilization (e.g., from shallow soil reservoirs), or dilution (common for geogenically derived solutes), respectively (Knapp et al., 2020; Musolff et al., 2015; Zhi et al., 2020). This analysis was applied across the whole data-set (which was log-transformed prior to analysis), and broken down for each water year (2016–2021).

Snowmelt-driven hydrological events shunt a large fraction of annual terrestrial solute discharge to rivers and streams (Raymond et al., 2016). To better identify the sources of snowmelt-driven solutes we examined the cQ relationship associated with the rising and falling limb of the snowmelt hydrograph. The onset of the rising limb

was identified by a monotonic increase in Q of a magnitude double that of the monthly averaged baseflow Q. Similarly, the falling limb represented the sustained period of decreasing Q that followed the peak Q for each year.

We also calculated the coefficient of variation of solute concentration (CV_c) and discharge (CV_q) (Basu et al., 2011; Knapp et al., 2022; Thompson et al., 2011). Analysis of this ratio between concentration and discharge (CV_c/CV_q) can further explore whether the underlying relationship in solute export is driven by variability in discharge, improving understanding of solute mobilization (Knapp et al., 2022). For example, a CV_c/CV_q ratio ≤0.5 indicates that the variability in discharge (CV_q) is greater than the variability in solute concentrations (CV_c), and is therefore, chemostatic. By contrast, high solute concentration variability relative to discharge ($CV_c/CV_q \geq 0.5$) might be considered chemodynamic. We calculated the coefficient of variation using a previously published approach for log-normal data (Knapp et al., 2022),

$$CV = \frac{\sigma}{\mu} = \frac{exp(\mathrm{m} + 0.5s^2)}{exp(2m + s^2)\,(exp(s^2) - 1)} = \sqrt{exp(s^2) - 1} \quad (1)$$

where m and s represent the mean and standard deviation of the data.

2.6. Causality Analysis With Information Theory

To contextualize watershed nitrate export alongside the factors determining transit and loss through the watershed we treat the time series of different hydrological, physical, biogenic, and geogenic data (from 2016 to 2021) as a coupled process network (Ruddell & Kumar, 2009). Herein, the directional impacts from one process (e.g., geogenic leaching, or snowmelt) to the other (e.g., nitrate export) is quantitatively inferred by Shannon information entropy (H, Equation 2) and its transfer (TE, Equation 3) (unit: bits).

$$H = -\sum_{i=1}^{n} p(x_i)\, log_2\, p(x_i) \quad (2)$$

$$T_{X->Y} = \sum_{y_i, y_{i-1}, x_{i-j}} p(y_i, y_{i-1}, x_{i-j})\, log_2 \frac{p(y_i \mid y_{i-1}, x_{i-j})}{p(y_i \mid y_{i-1})} \quad (3)$$

where $p(x)$ is probability density function (PDF) of xi, $p(y_i,y_{i-1},x_{i-j})$ is the joint PDF of current time step y_i, previous time step of y_i, and jth time step before that, of x_i. $p(y_i|y_{i-1},x_{i-j})$ and $p(y_i|y_{i-1})$ denote conditional PDFs of the corresponding variables. For example, the information entropy transfer from snowmelt to nitrate export is calculated as Shannon entropy reduction (uncertainty reduction) of present nitrate export given the historical snowmelt records with a 12-month time lags, which means that we consider snowmelt dynamics of the previous year.

The TE approach measures the reduction of uncertainty in one time series due to the knowledge gained from another time series. However, to ensure the calculated TE does not stem from randomness we compare the statistical significance of the initial TE X→Y relationship (e.g., $TE^{SWE} -> NO_3^{EXPORT}$) with that following the random shuffling of the time series (Yuan et al., 2022). Specifically, we randomly shuffled the X and Y time series 10 times. Each time we generate new relationships and use Equation 3 to calculate the TE. If the original (X→Y) TE is lower than this new relationship, it is assigned a value of zero, indicating no causal relationship between X→Y. We report causality only when the X→Y of the original time series data is larger than its significance threshold.

We applied this causality modeling approach to the observed time series of watershed variables at both the Coal Creek and ERP. The factors included in the analysis were chosen as proxies for the different sources contributing stream NO_3^-, and included biogenic solutes derived from shallower soils (e.g., DOC), or deeper bedrock derived solutes (e.g., Mg^{2+}), redox active compounds (e.g., SO_4^{2-}), and hydrological variables influencing nutrient flux and riverine turnover (e.g., SWE and water temperature). Their relevance to NO_3^- was visualized in a network (Bastian et al., 2009) from which quatiative associations between different variables can be identified. The time-series of observations required daily, or near daily, collection frequency to be included in the analysis. Therefore,

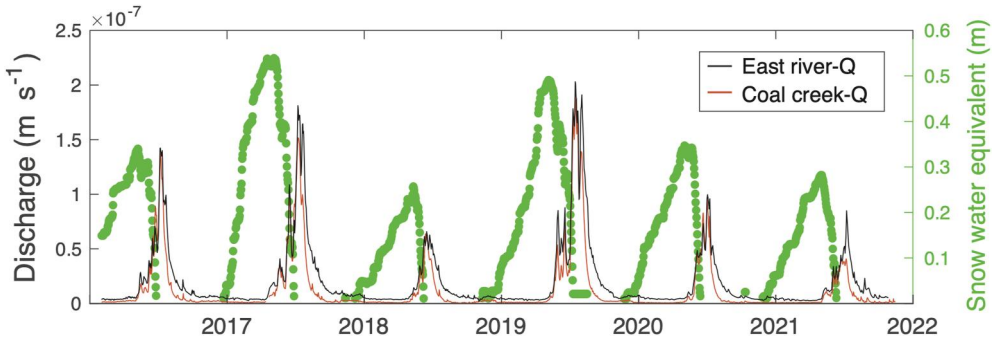

Figure 2. Discharge, and snow water equivalent throughout the study period (2016–2021). River discharge (m s^{-1}) data depicts both the Coal Creek and ERP catchments and is normalized by the areal extent of each catchment. Snow water equivalent (m) is derived from the SNOTEL station (Site 380).

while the seasonality and magnitude of atmospheric deposition are likely relevant to NO_3^- export, poor temporal resolution in collection precluded its inclusion here.

2.7. Assessment of Annual and Snowmelt Nitrate Export

We calculated a time-series of total mass yields leaving the Coal Creek and ERP catchments *Y(t)* (kg ha^{-1} yr^{-1}) using the discharge, *Q(t),* and concentration, *C(t),* time series by integrating from day 1 of each water year to day 365 for annual time series, and during the snowmelt periods (Equation 4). The mass export is the multiplication of discharge *Q(t)* (m^3/s) and concentration of nitrate *C(t)* (in kg/m^3) and summed for all daily time steps (dt):

$$Yields = Y(t) = \sum_{day\ 1}^{day\ 365} \frac{Q(t)\,C(t)\,dt}{Area} \tag{4}$$

Discharge and concentration time series were gap-filled and interpolated using a simple averaging method where missing values were replaced by a rolling average of the previous and subsequent day's concentration. We relate solute fluxes from inputs (e.g., atmospheric deposition) to the riverine outputs through Equation 5 which describes the retention of N within each watershed on a water year basis:

$$Retention\ Capacity = Ret\% = \frac{Deposition - Yields}{Deposition} * 100 \tag{5}$$

3. Results

3.1. Concentration-Discharge Behavior

The time span of this study covered both historical highs and lows of discharge (Q, m s^1) and snow water equivalent (SWE, m) within Coal Creek and ERP. Both 2017 and 2019 were above average snowpack depth and discharge, while 2018 represented a historic low. Figure 2 provides the time course of SWE for the East River Watershed, and Q for both catchments. While the temporal trends in snowmelt driven discharge were similar between Coal Creek and ERP, the larger drainage area and lower proportion of forest coverage means that the streamflow was much higher within the ERP.

The annual average atmospheric deposition of nitrogen and NO_3^-, after accounting for catchment areal extent (Equations 4 and 5), was similar within Coal Creek (TN: 2.34 kg ha^{-1} yr^{-1} ± 0.21; NO_3^-: 1.03 kg ha^{-1} yr^{-1} ± 0.12) relative to ERP (TN: 2.67 kg ha^{-1} yr^{-1} ± 0.25; NO_3^-: 0.93 kg ha^{-1} yr^{-1} ± 0.12) (Table 1, Table S2, Figure S2 in Supporting Information S1). Despite similar deposition magnitudes, the annual riverine export of NO_3^- was 3.5x lower from Coal Creek (0.06 kg ha^{-1} yr^{-1} ± 0.02) than from ERP (0.21 kg ha^{-1} yr^{-1} ± 0.14). We further calculated the release of NO_3^- associated with snowmelt, by summing the concentration released during the rising and falling limb of discharge. Relative to total annual export, snowmelt

Table 1
Annual Nitrate Export Magnitudes Between East River and Coal Creek

		2016	2017	2018	2019	2020	2021	Average (std. dev)
East River	Annual NO_3^- export (kg ha^{-1} yr^{-1})	0.45	0.13	0.07	0.33	0.15	0.15	0.21 (0.14)
	Q Yield (km^3)	0.05	0.07	0.03	0.09	0.04	0.03	0.05 (0.02)
	Atm. NO_3^- deposition (kg ha^{-1} yr^{-1})	1.02	1.08	0.86	0.75	0.86	0.99	0.93 (0.12)
	Total N dep. (kg ha^{-1} yr^{-1})	2.67	2.71	2.35	2.28	2.69	2.96	2.61 (0.25)
Coal Creek	NO_3^- annual export (kg ha^{-1} yr^{-1})	0.06	0.06	0.02	0.096	0.05	0.052	0.06 (0.024)
	Q Yield (km^3)	0.02	0.03	0.01	0.03	0.02	0.01	0.02 (0.01)
	Atm. NO_3^- deposition (kg ha^{-1} yr^{-1})	1.15	1.16	0.94	0.87	0.95	1.09	1.03 (0.12)
	Total N dep. (kg ha^{-1} yr^{-1})	2.43	2.4	2.1	2.18	2.43	2.7	2.34 (0.21)

Note. These calculations use gap-filled data and are expressed as a function of the size of each watershed. Annual NO_3^- flux (kg ha^{-1} yr^{-1}) is calculated from Equation 4 at the water year time scale. Q yield (km^3) is the total volume of water that exited the watershed for each water year. Atm. NO_3^- deposition represents the total (i.e., wet + dry) nitrate deposition (kg-N/ha).

was responsible for the bulk of solute export, accounting for 80%–90% and 50%–90% of total NO_3^- export in Coal Creek and ERP, respectively.

The riverine NO_3^- concentrations spanned a similar order of magnitude within both the Coal Creek and ERP (Figures 3a–3i), and showed similar variability in concentration over the full range of Q. However, the CV_c/CV_q analysis indicates that both catchments show evidence of chemodynamic behavior ($CV_c/CV_q > 0.5$). When considered as independent water years (2016–2021), Coal Creek shows slightly more conservative behavior, with two years of overall chemostasis and the remainder chemodynamic. The CV_c/CV_q for the ERP showed stronger positive chemodynamic behavior across multiple years relative to Coal Creek, in contrast to the cQ data. For both Coal Creek and ERP, this analysis shows the importance of heterogeneous sources contributing to the aggregate export signal at different times of the year.

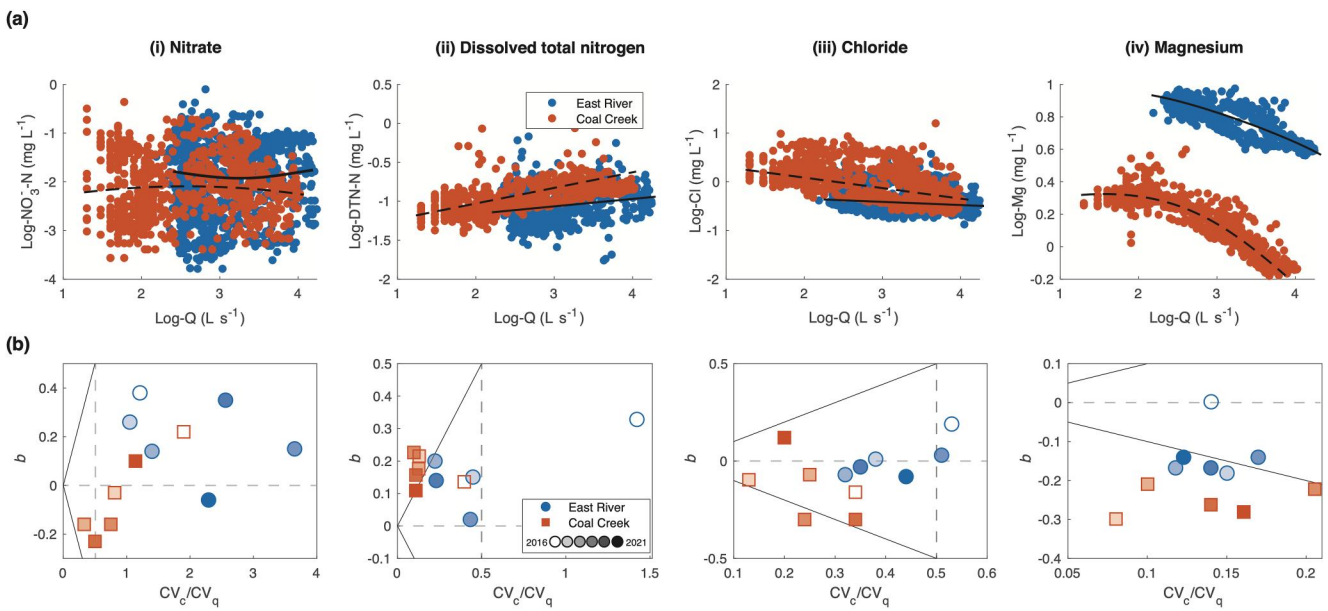

Figure 3. (a) Concentration-discharge relationships for different solutes within the ERP and Coal Creek catchments (i) nitrate, (ii) dissolved total nitrogen, (iii) chloride, and (iv) magnesium. Also shown are the lines of best fit, the slope of which is represented in the power law relationship as exponent b ($c = aQ^b$). (b) The ratio between the coefficient of variation for solute concentration and discharge (CV_c/CV_q) plotted against the exponent (b) of the power law relationship for the same solutes as in (a). Each plot depicts data for each water year. The different years (2016–2022) are shaded sequentially (from opaque to fully transparent). Also depicted in these plots are the positive and negative linear relationship between CV_c/CV_q and b (solid black lines), and the threshold point (at $CV_c/CV_q = 0.5$, dotted line) separating chemostatic from chemodynamic regimes.

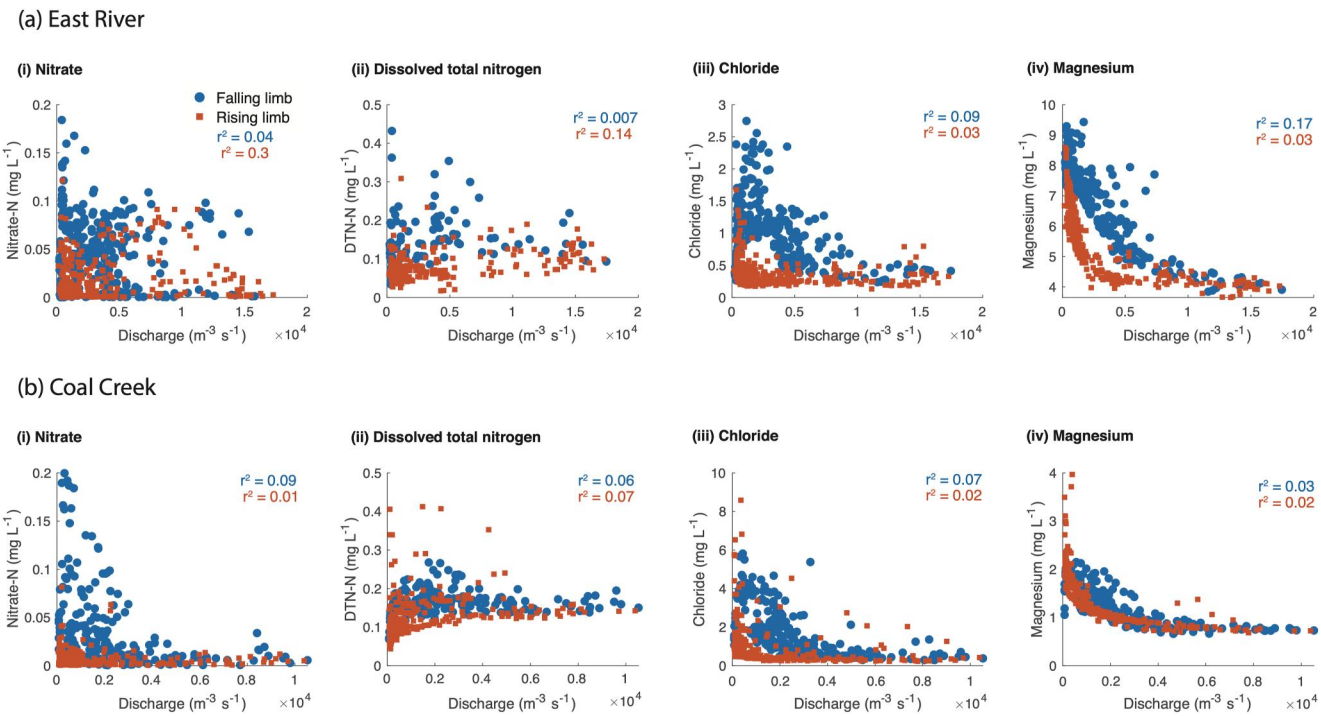

Figure 4. Relationship between the concentration of different nitrogen species (NO_3^-, DON), chloride, and magnesium, relative to the discharge for (a) the East River catchment, and (b) Coal Creek. The hydrograph is divided into the rising limb (increasing during the annual snowmelt period), and the falling limb (decreasing to baseflow).

Distinct behavior emerges during the rising and falling limb (Figure 4 and Table 2). The rising limb has little impact on riverine NO_3^- in either Coal Creek ($b = 0.1$), or the ERP ($b = 0.05$). However, the falling limb of the snowmelt period flushes NO_3^- into the ERP ($b = -0.6$), as the groundwater table reaches into the shallower soils. This impact is much weaker in Coal Creek ($b = -0.06$).

Riverine DTN cQ analyses showed a weakly increasing concentration with increasing Q for both Coal Creek ($b = 0.16$) and ERP ($b = 0.07$). Given that riverine NH_4^+ was extremely low (generally non-detectable, and always <1 μM, Figure S3 in Supporting Information S1), the DTN measurements likely reflect the export of dissolved organic nitrogen in these systems. The observed behavior was also apparent under the falling limb in the ERP, and under increasing and decreasing Q in Coal Creek (Table 2). However, the CV_c/CV_q ratio was typically low (<0.5) for both Coal Creek and the ERP, indicating little relationship between DTN export and Q.

Chloride (Cl^-) export was reported here as a putative conservative tracer of watershed export processes and showed broad chemostatic behavior with Q in ERP ($b = -0.02$, with an interannual range = −0.08–0.19), and in Coal Creek ($b = -0.07$, interannual range = −0.3–0.12). In general, riverine Cl^- concentrations decreased with Q during snowmelt (Figure 4), but the CV_c/CV_q ratio demonstrated a longer-term chemostasis (Figure 3b).

Table 2
Exponent b for the Concentration-Discharge of Various Elements

	East river	Coal creek
Nitrate	0.013 (−0.06/0.38)	−0.01 (−0.23/−0.2)
Dissolved total nitrogen	0.07 (−0.02/0.37)	0.16 (0.11/0.2)
Chloride	−0.02 (−0.08/0.19)	−0.07 (−0.3/0.12)
Magnesium	−0.14 (−0.18/0)	−0.26 (−0.3/−0.21)

Note. The table provides the value calculated from the complete data set. In brackets are the ranges in *b* spanned by individual years (2016–2021).

The cQ relationship for magnesium provides insight into the export behavior of a predominantly bedrock-derived solute. Riverine Mg^{2+} concentration was far higher in the ERP where soils are underlain by a Cretaceous Mancos shale bedrock, yet the trajectory of Mg^{2+} export was similar between the catchments and generally showed a non-linear decline in concentration under increasing Q (Figures 3a and 4). CV_c/CV_q ratios generally support the observations from cQ slopes, with geogenically derived solutes showing little variability in concentrations, and are strongly driven by changes in discharge (Fox et al., 2022).

Causality analysis, through transfer entropy (Ruddell & Kumar, 2009), was used to further parse out the factors regulating NO_3^- transit and export

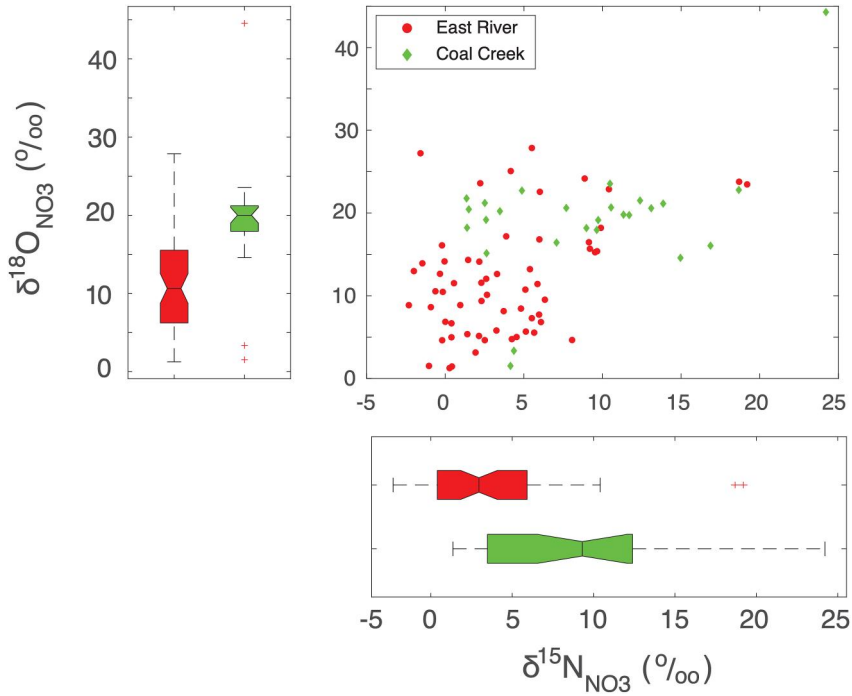

Figure 5. Biplot depicting the relationship between $\delta^{15}N_{NO3}$ and $\delta^{18}O_{NO3}$ within streamwater collected within Coal Creek and the ERP.

(Figures S4a and S4b in Supporting Information S1). SWE and water temperature were important factors governing export from both catchments (Figure S4c in Supporting Information S1). However, biogenic, and to a lesser extent geogenic, variables were closely associated with NO_3^- release to streams within the ERP, indicating the contribution of both shallow and deep sources to the NO_3^- aggregate flux. By contrast, NO_3^- exported from Coal Creek showed no direct connection to biogenic or geogenic export (Figure S4c in Supporting Information S1), potentially indicating a larger role for the direct transfer of atmospheric NO_3^- to stream NO_3^- export.

3.2. Streamwater $\delta^{15}N_{NO3}$ and $\delta^{18}O_{NO3}$

The isotopic composition of NO_3^- ($\delta^{15}N_{NO3}$ and $\delta^{18}O_{NO3}$) in stream water within Coal Creek and the ERP was measured across a two-year period between 2019 and 2021, capturing historic highs and lows in snowpack depth and streamflow (Figure S5 in Supporting Information S1). The lower NO_3^- concentrations within Coal Creek (<2 μM) precluded isotopic measurements during much of the baseflow period, and measurements focused mainly on the snowmelt period. The $\delta^{15}N_{NO3}$ within the ERP showed a narrower range of values than Coal Creek. In the ERP $\delta^{15}N_{NO3}$ spanned −2.3–19.2‰ (3.8 ± 4.4‰, mean and standard deviation), and 1.4–24‰ (8.9 ± 6‰) in Coal Creek. Similarly, $\delta^{18}O_{NO3}$ ranged from 1.2 to 27.8‰ (11.8 ± 6.8‰) in the ERP, and 1.5–44.5‰ (19.3 ± 7.3‰) in Coal Creek (Figure 5).

3.3. Sources of Exported Nitrate

We used a simple mixing model to determine the contributions of atmospheric and soil-/saprolite-derived NO_3^- to aggregate NO_3^- export. The atmospheric component of this mixing model was derived from measurements of the isotopic composition of precipitation from both Coal Creek and ERP. The isotopic signal of both snow and rainfall was similar between the two catchments, showing an average (± standard deviation) $\delta^{15}N_{NO3}$ of 6.4 ± 4.3‰ and 18.6 ± 5‰ and a $\delta^{18}O_{NO3}$ average of 73 ± 11.1‰ and 65.6 ± 9.6‰, for rainfall and snowfall respectively (Figure S6 in Supporting Information S1). The soil-derived signal, attributable to nitrification, was calculated from a $\delta^{18}O$ value of O_2, and the measured values for $\delta^{18}O$ from porewater sampled from the hillslope boreholes. The specific approach for estimating the $\delta^{18}O$ values of nitrification can be found in the supplemental material and methods. Measurements of dissolved NO_3^- were not made for Coal Creek soils, so mixing model calculations were made using nitrification data derived from ERP soils, which overlap with previously published

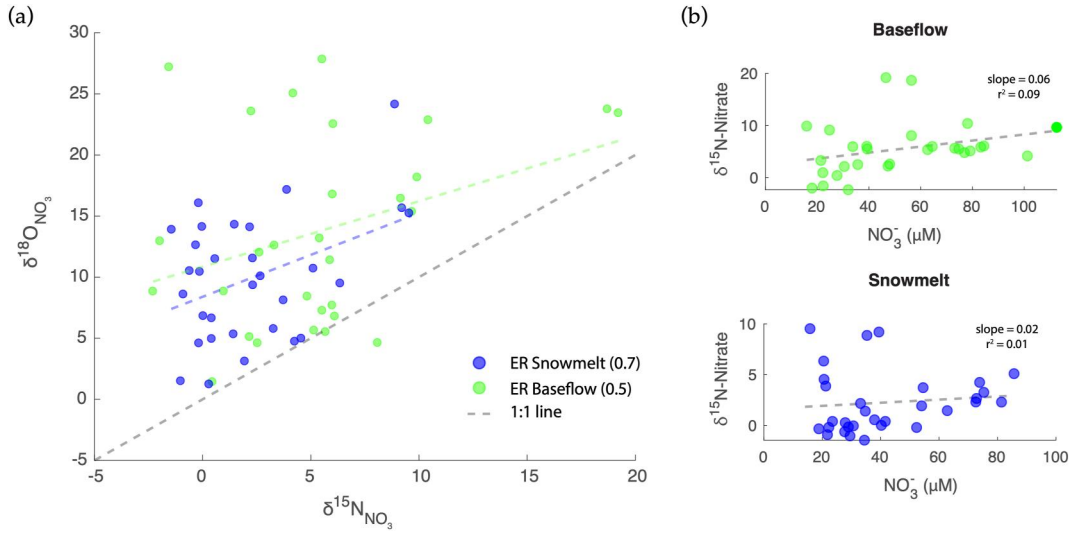

Figure 6. (a) Biplot showing the relationship between $\delta^{15}N_{NO3}$ and $\delta^{18}O_{NO3}$ in the East River during distinct periods of the hydrograph, snowmelt and baseflow, while (b) depicts the relationship between nitrate concentrations and $\delta^{15}N_{NO3}$.

values (Granger & Wankel, 2016). This mixing model demonstrated that a large fraction of riverine NO_3^- exported from Coal Creek was derived directly from atmospheric deposition (~41%), with the remainder sourced from soil pools. The range of atmospheric contributions to NO_3^- export in Coal Creek varied from 20% to 62% (Table S3 in Supporting Information S1). A weighted approach to calculating the percent contribution of atmospheric sources to distinct periods of the hydrograph shows it to be larger during the snowmelt period (34 ± 5%) relative to baseflow (20 ± 4%) (Table S3 in Supporting Information S1). By contrast, the majority of exported NO_3^- from the ERP was derived from nitrification (~82%), with the direct contribution from atmospheric NO_3^- deposition ranging across the year from 16% to 29%. While ERP showed high variability of $\delta^{18}O_{NO3}$ throughout the year, the percent contribution of atmospheric NO_3^- to export was similar for the snowmelt (22 ± 3%), and baseflow period (24 ± 7%) (Table S3 in Supporting Information S1). The $\Delta\delta^{18}O_{NO3}$: $\Delta\delta^{15}N_{NO3}$ trajectory showed a linear relationship with a slope of 0.7 and 0.5, during snowmelt and baseflow respectively (Figure 6a), which would be expected for residual NO_3^- that had been partially denitrified (Burns et al., 2009). Plotting $\delta^{15}N_{NO3}$ against NO_3^- concentrations (Figure 6b), also emphasized the mixing of different water and NO_3^- sources during different periods of the hydrograph.

3.4. Terrestrial Nitrate Cycling in the East River

To strengthen understanding of how different sources and sinks contribute to the aggregate NO_3^- export within the ERP catchment, we developed a depth-resolved, time series of $\delta^{15}N_{NO3}$ and $\delta^{18}O_{NO3}$ across a hillslope-toeslope-floodplain transect. This time series permits the identification of major source-sink hotspots across the terrestrial system that could account for the stronger biogeochemical processing of nitrogen within the ERP. Moreover, the time period of intensive sampling encompassed the same event driven trajectory as the riverine data, capturing historic high and low snowpack depths.

Analysis of the $\Delta\delta^{18}O_{NO3}$: $\Delta\delta^{15}N_{NO3}$ trajectories across the transect, and the wide range of isotopic values, show persuasive evidence for both actively fractionating mechanism (e.g., denitrification, NO_2^- reoxidation) and mixing of different sources at each sampling location. Surface soils (i.e., top 30 cm) on the hillslope showed a $\delta^{15}N_{NO3}$ range of −0.3–16.7‰ (4.2 ± 3.2‰, mean and standard deviation) and −10.7–4‰ (−4.3 ± 3.5‰) for $\delta^{18}O_{NO3}$. $\delta^{15}N_{NO3}$ within the hillslope weathering zone ranged from 0.4–26.8‰ (6 ± 4.8‰) and −10.8–14.1‰ (−3.3 ± 5.4‰) for $\delta^{18}O_{NO3}$. Both of these depths showed a linear relationship between the $\Delta\delta^{18}O_{NO3}$: $\Delta\delta^{15}N_{NO3}$ of 0.5 and 0.65 (Figure 7a) that indicates NO_3^- loss via an actively fractionating mechanism, but also shows evidence of mixing of different source waters overprinting on this relationship (Figure 7b).

The surface soils of the toeslope ($\delta^{15}N_{NO3}$: 6.3 ± 2.7‰ mean std dev, range: 3.5–10.7‰; $\delta^{18}O_{NO3}$ −0.9 ± 6.7‰, −8.5–8.1‰) and the floodplain ($\delta^{15}N_{NO3}$: 1.3 ± 7.3‰ mean std dev, range: −6.8–16.5‰; $\delta^{18}O_{NO3}$

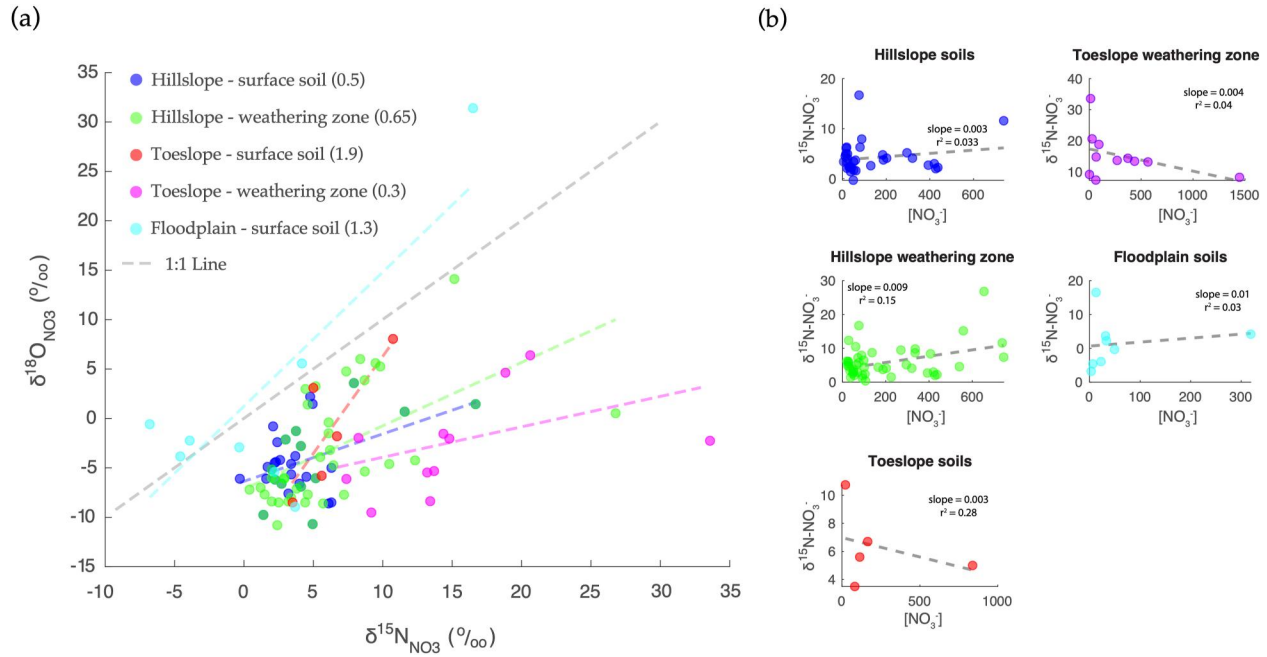

Figure 7. Nitrate isotopes within the terrestrial subsurface across a hillslope transect in the East River catchment. (a) Relationships between $\delta^{15}N_{NO3}$ and $\delta^{18}O_{NO3}$ across the hillslope-toeslope-floodplain transect. The slope of that relationship is provided in brackets. (b) $\delta^{15}N_{NO3}$ plotted against the concentration of NO_3^-.

1.6 ± 12.7‰, −8.9–31.4‰) showed a $\Delta\delta^{18}O_{NO3}$: $\Delta\delta^{15}N_{NO3}$ trajectory that deviated positively from the 1:1 line (Figure 7a), indicating elevated rates of NO_2^- reoxidation, relative to NO_3^- reduction, contributing to the NO_3^- pool. Finally, the weathering zone of the toeslope region ($\delta^{15}N_{NO3}$: 13.9 ± 8.4‰ mean std dev, range: −1.5–33.6‰; $\delta^{18}O_{NO3}$ -0.8 ± 8.6‰, −9.5–21.9‰) also showed a positive $\Delta\delta^{18}O_{NO3}$: $\Delta\delta^{15}N_{NO3}$ trajectory, albeit at a shallower relationship (0.3) than might be expected solely from the contribution of NO_3^- reduction (Figure 7a), which might also be due to mixing of different water sources (Figure 7b).

4. Discussion

4.1. Riverine Nitrate Export

Gradients in vegetation, topography, geology, and geomorphology all play critical roles in determining nitrogen availability, and regulating its retention and release from headwaters (Bormann & Likens, 1967; Sebestyen et al., 2014, 2019). Paired catchment studies are important approaches to improve understanding of the role distinct geophysical and ecological traits play in the transformation of nitrogen while controlling for climatic properties, and the magnitude of nitrogen deposition (Schiff et al., 2002). When normalized to catchment area, the ERP exported ∼3.5x as much NO_3^- as Coal Creek (0.21 ± 0.14 kg ha^{-1} yr^{-1} from ERP, relative to 0.06 ± 0.02 kg ha^{-1} yr^{-1} from Coal Creek. Table 1 and Figure 8). The ERP is the larger catchment; however, nitrate deposition was calculated to be similar (0.93 ± 0.12 kg ha^{-1} yr^{-1} in ERP, relative to 1.03 ± 0.12 kg ha^{-1} yr^{-1} in Coal Creek), indicating that Coal Creek retained more atmospherically deposited NO_3^- (∼94%) than ERP (∼77%). This is consistent with previous observations of high NO_3^- retention within forested catchments (Campbell et al., 2004; Groffman et al., 2004; Wexler et al., 2014), where recycling of internal soil nitrogen pools sustains nitrogen demand (Fahey et al., 1985; Gosz, 1981), and reduces NO_3^- export from the catchment.

Riverine concentration-discharge relationships (i.e., cQ and CV_c/CV_q) provide insight as to how catchments store and release solutes (Knapp et al., 2022). Cl^- and Mg^{2+} displayed characteristic relationships with increasing discharge in both ERP and Coal Creek. Cl^- shows consistent chemostatic behavior with increasing discharge (Figure 3), which might be expected for a predominantly atmospherically deposited solute. However, Cl^- can deviate from this conservative behavior (Svensson et al., 2012) due to, for example, evapoconcentration under dry conditions or complexation with soils and vegetation (Lovett et al., 2005; Myneni, 2002) resulting in event-drive

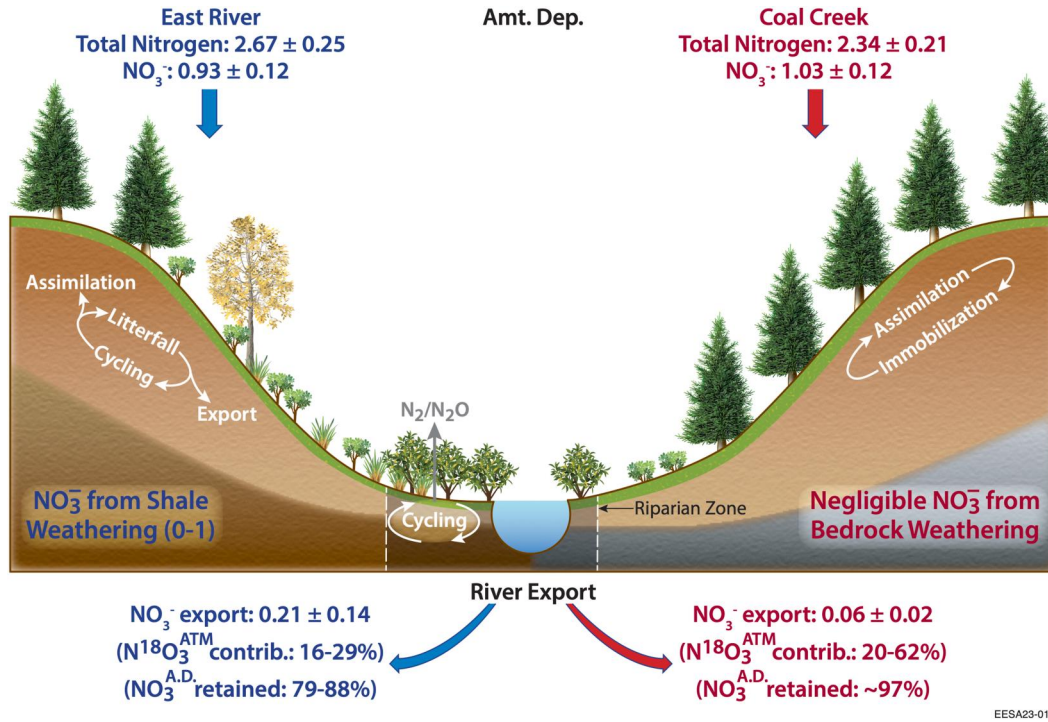

Figure 8. Schematic representation of the differential retention of NO_3^- (in kg ha^{-1} yr^{-1}) across the two catchments as a function of their distinct vegetation and bedrock properties. Also provided are the direct contribution of atmospherically deposited nitrate ($N^{18}O_3^{ATM}$) to exported NO_3^-, the percentage of atmospherically deposited NO_3^- retained in different watersheds, and the percentage of atmospherically deposited nitrate (NO_3^{AD}) retained in the catchment. Estimates for the magnitude of atmospheric deposition of nitrogen and NO_3^- and the contribution of shale bedrock weathering (ERP only) are also provided.

mobilization (Knapp et al., 2020). However, within ERP or Coal Creek, Cl^- concentrations generally declined under the falling limb of snowmelt (Figure 4), suggesting supply limitation consistent with atmospheric deposition controlling riverine Cl^- export patterns. Mg^{2+} concentrations declined with increasing discharge, indicating solute export limited by supply, consistent with the activation and release of organic-poor, geogenic sources of solutes (Zhi et al., 2019). However, both catchments showed large variability in NO_3^- concentrations across the measured range in discharge (Figures 3a and 3b), indicating the contribution of multiple sources of terrestrial NO_3^- to the aggregate downstream export profile (Thompson et al., 2011).

A causality analysis, used to identify the interacting network of factors influencing NO_3^- export (Ruddell & Kumar, 2009), showed SWE and water temperature were important, interdependent factors driving NO_3^- export in Coal Creek and ERP. Snowmelt is the dominant period of NO_3^- export for both of these catchments, accounting for over 80% of export in Coal Creek, and over 50% for ERP, consistent with studies in other mountainous regions (Brooks et al., 1999; Petrone et al., 2007; Sickman et al., 2003; although see Hall et al., 2016). We also identified factors contributing to NO_3^- export that were unique to each catchment. Export in the ERP is strongly related to biogenic (e.g., microbial turnover of DOC, which can be tied to NO_3^- reduction) and geogenic (e.g., bedrock weathering) processes (Figure S4 in Supporting Information S1) when compared with Coal Creek. The coupling between biogenic solutes and NO_3^- export in this analysis suggests mobilization of shallower soil solutes (including DOC and NO_3^-) as water tables rise through the soil profile and connectivity between shallow soils and the river is established (Zhi & Li, 2020). Indeed, we observed NO_3^- export to increase with discharge on the falling limb (Figure 4), as the water table recedes from shallower soils.

Geogenic proxies showed strong information transfer with NO_3^- export in ERP (Figure S4 in Supporting Information S1), which is largely underlain by a nitrogen-rich Mancos Shale bedrock, which exhibits high snowmelt-driven weathering rates (Wan et al., 2019, 2020; Winnick et al., 2017) in some areas of the catchment. For example, Wan et al. (2020), estimated a base cation weathering rate for a hillslope within the ERP of 55.3 ± 4

$Kmol_c$ ha^{-1} yr^{-1}, and a shale-nitrogen release rate of 18.9 ± 4.4 kg ha^{-1} yr^{-1}, with a specific hillslope NO_3^- export of ~2.0 kg ha^{-1} yr^{-1}. The bulk of this geogenic NO_3^- is likely assimilated by plants or reduced by microbes within the floodplain, therefore, the contribution of geogenic sources of NO_3^- to the aggregate export signal remains uncertain. The high variability in riverine NO_3^- concentrations under baseflow conditions could represent the contribution of geogenic sources in the ERP, however, this variability is similar to that in Coal Creek (Figures 3a and 3b), which is underlain by crystalline igneous rocks containing only trace amounts of nitrogen (Holloway & Dahlgren, 2002). The high NO_3^- concentrations exported under low discharge in both catchments likely reflects the legacy storage, and subsequent mobilization, of groundwater NO_3^- (Johnson & Stets, 2020).

Estimating the contribution of bedrock NO_3^- to river exports is further complicated by the variability in the extent of weathered bedrock throughout the ERP catchment. The northeast-facing hillslope, where the bulk of our data was collected, shows high saprolite fracture density and a high weathering rate (Wan et al., 2020). However, other regions of the ERP, particularly toward the headwaters of the catchment, are underlain by older, harder shale, with fewer fractures (discussed further in Maavara et al., 2021), which are unlikely to release similar concentrations of nitrogen. At the catchment scale bedrock nitrogen likely contributes little to the total magnitude of watershed NO_3^- export, and we estimate a value between 0 and 1 kg ha^{-1} yr^{-1} for geogenic contributions to NO_3^- catchment export (Figure 8). By contrast, NO_3^- export in Coal Creek showed little to no information transfer between biogenic and geogenic processes, suggesting limited microbial transformation prior to export, and no contribution of bedrock weathering to NO_3^- export. In the following section we discuss measurements of the stable isotopes of NO_3^- to better constrain the different sources contributing to the aggregate export behavior of NO_3^- between the two catchments.

4.2. Riverine Nitrate Sources

He magnitude and seasonality of riverine NO_3^- export aggregates the sources and sinks that underpin NO_3^- mobilization from the terrestrial biosphere to the river. Measurements of $\delta^{15}N_{NO3}$ and $\delta^{18}O_{NO3}$ were, on average, higher in Coal Creek ($\delta^{15}N_{NO}$: 8.9 ± 6‰; $\delta^{18}O_{NO3}$: 19.3 ± 7.3‰) relative to the ERP ($\delta^{15}N_{NO}$: 3.8 ± 4.4‰; $\delta^{18}O_{NO3}$: 11.8 ± 6.8‰). While the range of $\delta^{15}N_{NO3}$ in both catchments were consistent with that from other subalpine rivers and lakes (Bourgeois et al., 2018; Hall et al., 2016; Nanus et al., 2008), the variance in these values supports the idea that the river NO_3^- signal is composed of multiple contributing sources, including snowmelt/precipitation, denitrification, and NO_2^- (re) oxidation (Granger & Wankel, 2016). However, broader trends in the data are also discernible.

Atmospheric deposition contributes a higher proportion of NO_3^- to Coal Creek export than in the ERP, with between 20% and 62% of exported NO_3^- stemming directly from deposition, compared with 16%–29% at ERP. A recent synthesis of riverine NO_3^- isotopes demonstrated the pervasive transport of unprocessed NO_3^- from forested catchments directly to the river, which tends to increase with snowmelt or stormflow periods that establish direct hydrological connectivity between terrestrial regions and the river (Sebestyen et al., 2019). A similar pattern was noted here for Coal Creek, whereby the majority of atmospheric NO_3^- was released during the snowmelt period (Table S3 in Supporting Information S1). By contrast, NO_3^- exported from the ERP was consistent with a predominant soil-derived source, indicating strong biological transformation of NO_3^- prior to hydrological loss. Previous paired catchment studies have demonstrated similar distinctions in NO_3^- export (Kelly et al., 2011), and the contrasting export sources described above can be related to the functional traits of the two catchments.

Higher proportions of atmospheric deposition contributing to NO_3^- export from Coal Creek might reflect the relatively small riparian region in that catchment. Riparian regions are important hotspots for nitrogen transfer (Pinay et al., 2018), and the narrower floodplain in Coal Creek would limit the potential for biogeochemical reactions to take place prior to export. However, plant-microbe interactions also play a critical role in shaping nutrient cycling on hillslopes adjacent to streams, and soils under mountainous conifer stands tend to be low in nitrogen due to high C: N litter (Leonard et al., 2020), high immobilization due to higher coarse woody debris (Lajtha, 2020), and low rates of mineralization and nitrification (Gosz, 1981). Such a conservative nitrogen cycle might thus contribute to higher losses of unprocessed nitrate from Coal Creek. Indeed, a comparison of the cQ relationships for NO_3^- and DTN (Figures 3 and 4) would also suggest the low accumulation of NO_3^- in organic-rich soils in Coal Creek. During the falling limb of snowmelt, DTN maintains a similar concentration as discharge

increases (Figure 4) suggesting mobilization as the water table recedes from shallow soils. NO_3^-, by contrast, declines with increasing discharge, indicating the limitation of supply in organic-rich soils.

By contrast, the ERP shows evidence of a more open nitrogen cycle, with lower $\delta^{15}N_{NO3}$ and $\delta^{18}O_{NO3}$ values indicating clear microbial processing prior to export of NO_3^-, is likely due to both the contribution of diverse vegetation (including montane species, Aspen glades, and conifer stands) with a higher rate of litter accumulation and turnover (Maavara et al., 2021), and the formation of biogeochemical hotspots across the landscape. Indeed, the $\Delta\delta^{18}O_{NO3}$: $\Delta\delta^{15}N_{NO3}$ trajectory at ERP showed evidence for the imprint of actively fractionating metabolisms (e.g., denitrification) during both snowmelt and baseflow periods (Figure 6a), concomitant with mixing of different sources (Figure 6b). To better constrain the major sources and sinks of NO_3^- contributing to this aggregate riverine signal, we measured the $\delta^{15}N_{NO3}$ and $\delta^{18}O_{NO3}$ of depth-resolved porewater samples across a hillslope-toeslope-floodplain transect adjacent to the ERP sampling station to identify hotspots of NO_3^- biogeochemistry within the terrestrial system.

4.3. Terrestrial Nitrate Cycling

$\Delta\delta^{18}O_{NO3}$: $\Delta\delta^{15}N_{NO3}$ trajectories within hillslope surface soils indicate the formation of temporal denitrification hotspots (Figure 7a). Previous work along this hillslope has recorded a pulse of extractable soil NO_3^- during the snowmelt period in surface soils (Sorensen et al., 2020). This pulse occurred due to snowmelt-driven lysis of microbial biomass built-up under the snowpack, and released both labile carbon and nitrogen, elevating rates of mineralization and nitrification (Sorensen et al., 2020). The elevated availability of NO_3^- combined with high soil moisture content during the snowmelt period could promote the formation of strong oxic/anoxic gradients in shallow soils on the hillslope, enabling the spatial and temporal coupling of aerobic (e.g., nitrifying) and anaerobic (denitrifying) metabolisms (Bouskill et al., 2019), and loss of NO_3^- as N_2O and N_2 (Wan et al., 2020).

Furthermore, within the hillslope weathering zone a mass balance calculation using subsurface NO_3^- cQ from the upper hillslope region to the toeslope suggests that much of the NO_3^- accumulating is subject to denitrification prior to export to the groundwater and floodplain (Wan et al., 2020). The isotopic measurements made within the saprolite regions support this ascertain: The isotopic composition of NO_3^- is consistent with a nitrification source, while the trend in $\Delta\delta^{18}O_{NO3}$: $\Delta\delta^{15}N_{NO3}$ follows a linear relationship of ~0.6 consistent with denitrification (Granger & Wankel, 2016). Hillslopes within snow dominated ecosystems can serve as a direct source of NO_3^- to the groundwater (Beegum et al., 2023) and to rivers through quickflow (Ohte et al., 2004), and while strong precipitation events (e.g., monsoonal periods) can do the same (Marinos et al., 2018), soil moisture monitoring across the hillslope has demonstrated that rainfall does not infiltrate deeply into the soils during monsoonal events (Tokunaga et al., 2022). As such, hydrologic connectivity between hillslopes and the groundwater during and after snowmelt (i.e., during the falling limb), likely mobilizes the residual NO_3^- from hillslope soils, contributing to the observed NO_3^- isotopic trends during these periods.

Further down the transect, into the toeslope and floodplain regions, NO_3^- isotopic composition and trends ($\Delta\delta^{18}O_{NO3}$: $\Delta\delta^{15}N_{NO3}$) showed evidence for mixing of different NO_3^- sources (Figures 7a and 7b). The data presented here provides little compelling evidence for the formation of biogeochemical hotspots within the riparian region adjacent to the stream. Following the initial event-driven flush of water, the water residence times in riparian regions are generally slow, allowing for biogeochemical transformations of nitrogen compounds (Lutz et al., 2020; Pinay et al., 2018), including coupled nitrification and denitrification (Bouskill et al., 2019), and dissimilatory nitrate reduction to ammonia (DNRA, Wang et al., 2020). Sparse data availability in these regions preclude the identification of strong relationships; however, this lack of isotopic data arose because the majority of porewater NO_3^- measurements were below detection limits, which, in itself, suggests a strong sink for NO_3^-. The mixing of different water and NO_3^- sources within depositional zones, including toeslopes and floodplains, can mask strong trends in $\Delta\delta^{18}O_{NO3}$: $\Delta\delta^{15}N_{NO3}$. Trends in $\Delta\delta^{18}O_{NO3}$: $\Delta\delta^{15}N_{NO3}$ that deviate positively from 1, as observed in the toeslope and floodplain are usually indicative of higher $\delta^{18}O_{H20}$ values incorporated into NO_3^- during the (re) oxidation of NO_2^- (Granger & Wankel, 2016). These higher values might occur due to low vapor pressure deficits in mountainous systems increasing evapo (transpiration) along the hillslope or within the floodplain, enriching the residual $\delta^{18}O_{H20}$ (Oerter et al., 2014).

The functional potential for denitrification was observed across several ERP floodplains (Carnevali et al., 2020), however, this area was also been shown to be a potential hotspot for DNRA (Carnevali et al., 2020). At the ecosystem scale, DNRA tends to function as a retention mechanism for nitrogen, which might be important in

nitrogen-limited ecosystems. However, the DNRA reactions fractionates the ^{15}N and ^{18}O of NO_3^- in a similar manner ($^{15}\varepsilon$:$^{18}\varepsilon$ = 0.5–1.0) to denitrifying bacteria (Asamoto et al., 2021), and, under certain conditions, can co-exist (Jia et al., 2020). Therefore, differentiating the contribution of denitrification and DRNA to NO_3^- cycling will likely require further measurements (e.g., Robertson et al., 2019). Rogers et al. (2021) modeled the hydrological and biogeochemical processes responsible for the retention and release of reactive nitrogen within the ERP riparian region. They concluded that these regions are major control points for river corridors, providing ~20% of the stream NO_3^-, but are also major sinks for NO_3^-, due to a combination of denitrification and DNRA. DNRA emerged as an important pathway for NO_3^- reduction within the floodplain, accounting for approximately a quarter of NO_3^- turnover, with denitrification accounting for the majority. This is consistent with previous studies showing similar proportions of NO_3^- reduction attributable to denitrification, but contrary to recent syntheses showing DNRA to dominate NO_3^- reduction in some riparian regions (Wang et al., 2020).

5. Conclusions

Nitrogen retention plays a critical role in maintaining ecosystem function in mountainous watersheds. Here, we combined several years of concentration-discharge behavior with NO_3^- isotopic data identifying different sources and sinks to better understand how catchments characterized by distinct trait distributions differ in their retention and release of nitrogen. We note that the conifer-dominated (Coal Creek) and montane-dominated (ERP) catchments exhibited generally similar cQ behavior, with strong variability in concentration across the range of discharge indicative of multiple sources contributing the aggregate riverine signal. Yet, Coal Creek (at 0.06 ± 0.02 kg ha^{-1} yr^{-1}) releases ~3.5 time less NO_3^- relative to ERP (0.21 ± 0.14 kg ha^{-1} yr^{-1}). When the analysis focused on distinct hydrological events during the snowmelt periods, the montane dominated catchment showed evidence for increasing export under the falling limb, which was absent in the conifer dominated catchment. This data broadly shows evidence for distinct nitrogen cycles emerging the two catchments due to the different collection of functional traits despite similar cQ behavior. The isotopic composition of NO_3^- further emphasized these distinctions, with ~29–62% of NO_3^- exported in Coal Creek being derived from atmospheric deposition. This likely stems from low organic mineralization and nitrification under conifer stands, reducing the mobilization of soil-derived NO_3^- as water tables fall, as well as the narrower riparian region reducing biogeochemical turnover of NO_3^- prior to export. Within the montane-dominated catchment, riverine NO_3^- derived primarily from export of soil nitrogen (~82%), and displayed a strong signal of microbial processing (e.g., nitrification/denitrification) prior to export. Interestingly, we identified the hillslope regions as critical control points for NO_3^- cycling, with evidence for both nitrification, and denitrification in shallow soils, and in weathering zone due to longer water residence times following snowmelt.

The terrestrial nitrogen cycle continues to undergo substantial perturbation (Steffen et al., 2015), including the reported onset of nitrogen oligotrophication in undisturbed catchments (Craine et al., 2018; Mason et al., 2022). Moreover, nitrogen-limited mountainous ecosystems face a higher rate of atmospheric warming, with the increased frequency of low-to no-snow winters exacerbating water limitation (Siirila-Woodburn et al., 2021). Clarifying the role distinct functional traits (including topography, bedrock weathering properties, soil properties, land cover, etc.) play in the retention and release of nitrogen is critical for developing a predictive understanding of the nitrogen cycle in mountainous systems. Paired catchment studies, that combine relatively cost-effective measurements of solute concentrations across the hydrograph, with more involved isotopic measurements, provide important information on the mechanisms underpinning solute behavior, and represent one prominent avenue for further constraining the trajectory of the nitrogen cycle.

Data Availability Statement

The data and scripts used to produce the figures are available publicly through https://data.ess-dive.lbl.gov/data via doi:10.15485/1660462, doi:10.15485/1660456. While streamflow and discharge data are available at doi:10.15485/1779721, and doi:10.21952/WTR/1495380.

Acknowledgments
This material is based upon work as part of the Watershed Function Scientific Focus Area supported by the U.S. Department of Energy, Office of Science, Office of Biological and Environmental Research under contract number DE-AC02-05CH11231. We thank the two reviewers for helpful comments on an earlier version of the manuscript.

References

Alexander, R. B., Boyer, E. W., Smith, R. A., Schwarz, G. E., & Moore, R. B. (2007). The role of headwater streams in downstream water Quality1: The role of headwater streams in downstream water quality. *JAWRA Journal of the American Water Resources Association*, *43*(1), 41–59. https://doi.org/10.1111/j.1752-1688.2007.00005.x

Asamoto, C. K., Rempfert, K. R., Luu, V. H., Younkin, A. D., & Kopf, S. H. (2021). Enzyme-specific coupling of oxygen and nitrogen isotope fractionation of the nap and nar nitrate reductases. *Environmental Science and Technology*, *55*(8), 5537–5546. https://doi.org/10.1021/acs.est.0c07816

Ascott, M. J., Gooddy, D. C., Wang, L., Stuart, M. E., Lewis, M. A., Ward, R. S., & Binley, A. M. (2017). Global patterns of nitrate storage in the vadose zone. *Nature Communications*, *8*(1), 1416. https://doi.org/10.1038/s41467-017-01321-w

Bastian, M., Heymann, S., & Jacomy, M. (2009). Gephi: An open source software for exploring and manipulating networks. *Proceedings of the International AAAI Conference on Web and Social Media*, *3*(1), 361–362. https://doi.org/10.1609/icwsm.v3i1.13937

Basu, N. B., Thompson, S. E., & Rao, P. S. C. (2011). Hydrologic and biogeochemical functioning of intensively managed catchments: A synthesis of top-down analyses: Managed catchments. *Water Resources Research*, *47*(10). https://doi.org/10.1029/2011WR010800

Beegumm, A., Malakar, A., Chittaranjan, R., & Snow, D. D. (2023). Importance of snowmelt on soil nitrate leaching to groundwater – a model study. *Journal of Contaminant Hydrology*, *255*, 104163. https://doi.org/10.1016/j.jconhyd.2023.104163

Berhe, A. A., & Torn, M. S. (2017). Erosional redistribution of topsoil controls soil nitrogen dynamics. *Biogeochemistry*, *132*(1–2), 37–54. https://doi.org/10.1007/s10533-016-0286-5

Bormann, F. H., & Likens, G. E. (1967). Small watersheds can provide invaluable information about terrestrial ecosystems. *155*, 7.

Bourgeois, I., Savarino, J., Caillon, N., Angot, H., Barbero, A., Delbart, F., et al. (2018). Tracing the fate of atmospheric nitrate in a subalpine watershed using $\Delta^{17}O$. *Environmental Science and Technology*, *52*(10), 5561–5570. https://doi.org/10.1021/acs.est.7b02395

Bouskill, N. J., Conrad, M. E., Bill, M., Brodie, E. L., Cheng, Y., Hobson, C., et al. (2019). Evidence for microbial mediated NO3− cycling within floodplain sediments during groundwater fluctuations. *Frontiers in Earth Science*, *7*, 189. https://doi.org/10.3389/feart.2019.00189

Brooks, P. D., Campbell, D. H., Tonnessen, K. A., & Heuer, K. (1999). Natural variability in N export from headwater catchments: Snow cover controls on ecosystem N retention. *Hydrological Processes*, *13*(14–15), 2191–2201. https://doi.org/10.1002/(sici)1099-1085(199910)13:14/15<2191::aid-hyp849>3.0.co;2-l

Campbell, D. H., Kendall, C., Chang, C. C. Y., Silva, S. R., & Tonnessen, K. A. (2002). Pathways for nitrate release from an alpine watershed: Determination using $\delta^{15}N$ and $\delta^{18}O$. *Water Resources Research*, *38*(5), 1–9. https://doi.org/10.1029/2001WR000294

Campbell, J. L., Hornbeck, J. W., Mitchell, M. J., Adams, M. B., Castro, M. S., Driscoll, C. T., et al. (2004). Input-output budgets of inorganic nitrogen for 24 forest watersheds in the northeastern United States: A review. Water, air. *and Soil Pollution*, *151*(1–4), 373–396. https://doi.org/10.1023/B:WATE.0000009908.94219.04

Carnevali, P. B. M., Lavy, A., Thomas, A. D., Crits-Christoph, A., Diamond, S., Meéheust, R., et al. (2020). Meanders as a scaling motif for understanding of floodplain soil microbiome and biogeochemical potential at the watershed scale (preprint). *Microbiology*. https://doi.org/10.1101/2020.05.14.086363

Carroll, R., Newman, A., Beutler, C., & Williams, K. (2021). *Stream discharge data collected within the East River*. Colorado for the Lawrence Berkeley.

Carroll, R. W. H., Gochis, D., & Williams, K. H. (2020). Efficiency of the summer monsoon in generating streamflow within a snow-dominated headwater basin of the Colorado river. *Geophysical Research Letters*, *47*(23). https://doi.org/10.1029/2020GL090856

Casciotti, K. L., & Buchwald, C. (2012). Insights on the marine microbial nitrogen cycle from isotopic approaches to nitrification. *Frontiers in Microbiology*, *3*. https://doi.org/10.3389/fmicb.2012.00356

Clark, S. C., Barnes, R. T., Oleksy, I. A., Baron, J. S., & Hastings, M. G. (2021). Persistent nitrate in alpine waters with changing atmospheric deposition and warming trends. *Environmental Science and Technology*, *55*(21), 14946–14956. https://doi.org/10.1021/acs.est.1c02515

Craine, J. M., Elmore, A. J., Wang, L., Aranibar, J., Bauters, M., Boeckx, P., et al. (2018). Isotopic evidence for oligotrophication of terrestrial ecosystems. *Nature Ecology & Evolution*, *2*(11), 1735–1744. https://doi.org/10.1038/s41559-018-0694-0

Fahey, T. J., Yavitt, J. B., Pearson, J. A., & Knight, D. H. (1985). The nitrogen cycle in lodgepole pine forests, southeastern Wyoming. *Biogeochemistry*, *1*(3), 257–275. https://doi.org/10.1007/BF02187202

Fox, P. M., Carrero, S., Anderson, C., Dewey, C., Keiluweit, M., Conrad, M., et al. (2022). Sulfur biogeochemical cycling and redox dynamics in a shale-dominated mountainous watershed. *Journal of Geophysical Research: Biogeosciences*, *127*(6). https://doi.org/10.1029/2021JG006769

Godsey, S. E., Kirchner, J. W., & Clow, D. W. (2009). Concentration-discharge relationships reflect chemostatic characteristics of US catchments. *Hydrological Processes*, *23*(13), 1844–1864. https://doi.org/10.1002/hyp.7315

Gomez-Velez, J. D., Harvey, J. W., Cardenas, M. B., & Kiel, B. (2015). Denitrification in the Mississippi River network controlled by flow through river bedforms. *Nature Geoscience*, *8*(12), 941–945. https://doi.org/10.1038/ngeo2567

Goodale, C. L. (2017). Multiyear fate of a ^{15} N tracer in a mixed deciduous forest: Retention, redistribution, and differences by mycorrhizal association. *Global Change Biology*, *23*(2), 867–880. https://doi.org/10.1111/gcb.13483

Gosz, J. R. (1981). Nitrogen cycling in coniferous forests. *Ecological Bulletins*, *30*, 405–426.

Granger, J., & Wankel, S. D. (2016). Isotopic overprinting of nitrification on denitrification as a ubiquitous and unifying feature of environmental nitrogen cycling. *Proceedings of the National Academy of Sciences*, *113*(42), E6391–E6400. https://doi.org/10.1073/pnas.1601383113

Groffman, P. M., Law, N. L., Belt, K. T., Band, L. E., & Fisher, G. T. (2004). Nitrogen fluxes and retention in urban watershed ecosystems. *Ecosystems*, *7*(4). https://doi.org/10.1007/s10021-003-0039-x

Hall, S. J., Weintraub, S. R., Eiriksson, D., Brooks, P. D., Baker, M. A., Bowen, G. J., & Bowling, D. R. (2016). Stream nitrogen inputs reflect groundwater across a snowmelt-dominated montane to urban watershed. *Environmental Science and Technology*, *50*(2), 1137–1146. https://doi.org/10.1021/acs.est.5b04805

Hobbie, E. A., & Högberg, P. (2012). Nitrogen isotopes link mycorrhizal fungi and plants to nitrogen dynamics. *New Phytologist*, *196*(2), 367–382. https://doi.org/10.1111/j.1469-8137.2012.04300.x

Holloway, J. A. M., & Dahlgren, R. A. (2002). Nitrogen in rock: Occurrences and biogeochemical implications: Biogeochemical implications of N in rock. *Global Biogeochemical Cycles*, *16*(4), 1–17. https://doi.org/10.1029/2002GB001862

Holloway, J. M., Dahlgren, R. A., Hansen, B., & Casey, W. H. (1998). Contribution of bedrock nitrogen to high nitrate concentrations in stream water. *Nature*, *395*(6704), 4–788. https://doi.org/10.1038/27410

Houlton, B. Z., Morford, S. L., & Dahlgren, R. A. (2018). Convergent evidence for widespread rock nitrogen sources in Earth's surface environment. *Science*, *360*(6384), 58–62. https://doi.org/10.1126/science.aan4399

Hubbard, S. S., Williams, K. H., Agarwal, D., Banfield, J., Beller, H., Bouskill, N., et al. (2018). The East river, Colorado, watershed: A mountainous community testbed for improving predictive understanding of multiscale hydrological–biogeochemical dynamics. *Vadose Zone Journal*, *17*(1), 1–25. https://doi.org/10.2136/vzj2018.03.0061

Jia, M., Winkler, M. K. H., & Volcke, E. I. P. (2020). Elucidating the competition between heterotrophic denitrification and DNRA using the resource-ratio theory. *Environmental Science and Technology*, *54*(21), 13953–13962. https://doi.org/10.1021/acs.est.0c01776

Johnson, H. M., & Stets, E. G. (2020). Nitrate in streams during winter low-flow conditions as an indicator of legacy nitrate. *Water Resources Research*, *56*(11). https://doi.org/10.1029/2019WR026996

Kelly, C. N., Schoenholtz, S. H., & Adams, M. B. (2011). Soil properties associated with net nitrification following watershed conversion from Appalachian hardwoods to Norway spruce. *Plant and Soil*, *344*(1), 361–376. https://doi.org/10.1007/s11104-011-0755-5

Knapp, J. L. A., Li, L., & Musolff, A. (2022). Hydrologic connectivity and source heterogeneity control concentration–discharge relationships. *Hydrological Processes*, *36*(9). https://doi.org/10.1002/hyp.14683

Knapp, J. L. A., von Freyberg, J., Studer, B., Kiewiet, L., & Kirchner, J. W. (2020). Concentration–discharge relationships vary among hydrological events, reflecting differences in event characteristics. *Hydrology and Earth System Sciences*, *24*(5), 2561–2576. https://doi.org/10.5194/hess-24-2561-2020

Kou, D., Yang, G., Li, F., Feng, X., Zhang, D., Mao, C., et al. (2020). Progressive nitrogen limitation across the Tibetan alpine permafrost region. *Nature Communications*, *11*(1), 3331. https://doi.org/10.1038/s41467-020-17169-6

Lajtha, K. (2020). Nutrient retention and loss during ecosystem succession: Revisiting a classic model. *Ecology*, *101*(1). https://doi.org/10.1002/ecy.2896

Lansdown, K., Heppell, C. M., Trimmer, M., Binley, A., Heathwaite, A. L., Byrne, P., & Zhang, H. (2015). The interplay between transport and reaction rates as controls on nitrate attenuation in permeable, streambed sediments: Nitrate removal in permeable sediments. *Journal of Geophysical Research: Biogeosciences*, *120*(6), 1093–1109. https://doi.org/10.1002/2014JG002874

Leonard, L. T., Mikkelson, K., Hao, Z., Brodie, E. L., Williams, K. H., & Sharp, J. O. (2020). A comparison of lodgepole and spruce needle chemistry impacts on terrestrial biogeochemical processes during isolated decomposition. *PeerJ*, *8*, e9538. https://doi.org/10.7717/peerj.9538

Li, D., Wrzesien, M. L., Durand, M., Adam, J., & Lettenmaier, D. P. (2017). How much runoff originates as snow in the western United States, and how will that change in the future? *Geophysical Research Letters*, *44*(12), 6163–6172. https://doi.org/10.1002/2017GL073551

Li, L., Sullivan, P. L., Benettin, P., Cirpka, O. A., Bishop, K., Brantley, S. L., et al. (2021). Toward catchment hydro-biogeochemical theories. *WIREs Water*, *8*(1). https://doi.org/10.1002/wat2.1495

Li, Y., Schichtel, B. A., Walker, J. T., Schwede, D. B., Chen, X., Lehmann, C. M. B., et al. (2016). Increasing importance of deposition of reduced nitrogen in the United States. *Proceedings of the National Academy of Sciences*, *113*(21), 5874–5879. https://doi.org/10.1073/pnas.1525736113

Lovett, G. M., Likens, G. E., Buso, D. C., Driscoll, C. T., & Bailey, S. W. (2005). The biogeochemistry of chlorine at Hubbard Brook, New Hampshire, USA. *Biogeochemistry*, *72*(2), 191–232. https://doi.org/10.1007/s10533-004-0357-x

Lutz, S. R., Trauth, N., Musolff, A., Van Breukelen, B. M., Knöller, K., & Fleckenstein, J. H. (2020). How important is denitrification in riparian zones? Combining end-member mixing and isotope modeling to quantify nitrate removal from riparian groundwater. *Water Resources Research*, *56*(1). https://doi.org/10.1029/2019WR025528

Maavara, T., Siirila-Woodburn, E. R., Maina, F., Maxwell, R. M., Sample, J. E., Chadwick, K. D., et al. (2021). Modeling geogenic and atmospheric nitrogen through the East River Watershed, Colorado rocky mountains. *PLoS One*, *16*(3), e0247907. https://doi.org/10.1371/journal.pone.0247907

Manning, A. H., Verplanck, P. L., Mast, M. L., & Wanty, R. B. (2008). *Hydrogeochemical investigation of the standard mine vicinity, upper Elk Creek basin, Colorado (scientific investigations report)*. USGS.

Marinos, R. E., Campbell, J. L., Likens, G. E., McDowell, W. H., & Rosi, E. J. (2018). Give and take: A watershed acid rain mitigation experiment increases baseflow nitrogen retention but increases stormflow nitrogen export. *Environmental Science and Technology*, *52*(22), 13155–13165. https://doi.org/10.1021/acs.est.8b03553

Mason, R. E., Craine, J. M., Lany, N. K., Jonard, M., Ollinger, S. V., Groffman, P. M., et al. (2022). Evidence, causes, and consequences of declining nitrogen availability in terrestrial ecosystems. *Science*, *376*(6590), eabh3767. https://doi.org/10.1126/science.abh3767

McDonnell, J. J., Sivapalan, M., Vaché, K., Dunn, S., Grant, G., Haggerty, R., et al. (2007). Moving beyond heterogeneity and process complexity: A new vision for watershed hydrology: Opinion. *Water Resources Research*, *43*(7). https://doi.org/10.1029/2006WR005467

Michalski, G., Bhattacharya, S. K., & Mase, D. F. (2012). Oxygen isotope dynamics of atmospheric nitrate and its precursor molecules. In M. Baskaran (Ed.), *Handbook of environmental isotope geochemistry* (pp. 613–635). Springer Berlin Heidelberg. https://doi.org/10.1007/978-3-642-10637-8_30

Moyes, A. B., Kueppers, L. M., Pett-Ridge, J., Carper, D. L., Vandehey, N., O'Neil, J., & Frank, A. C. (2016). Evidence for foliar endophytic nitrogen fixation in a widely distributed subalpine conifer. *New Phytologist*, *210*(2), 657–668. https://doi.org/10.1111/nph.13850

Musolff, A., Schmidt, C., Selle, B., & Fleckenstein, J. H. (2015). Catchment controls on solute export. *Advances in Water Resources*, *86*, 133–146. https://doi.org/10.1016/j.advwatres.2015.09.026

Myneni, S. (2002). Formation of stable chlorinated hydrocarbons in weathering plant material. *Science*, *295*(5557), 1039–1041. https://doi.org/10.1126/science.1067153

Nanus, L., Williams, M. W., Campbell, D. H., Elliott, E. M., & Kendall, C. (2008). Evaluating regional patterns in nitrate sources to watersheds in national parks of the rocky mountains using nitrate isotopes. *Environmental Science and Technology*, *42*(17), 6487–6493. https://doi.org/10.1021/es800739e

National Laboratory (2020). Watershed function science Focus area (water years 2019 to 2020). [Dataset]. https://doi.org/10.15485/1779721

Oerter, E., Finstad, K., Schaefer, J., Goldsmith, G. R., Dawson, T., & Amundson, R. (2014). Oxygen isotope fractionation effects in soil water via interaction with cations (Mg, Ca, K, Na) adsorbed to phyllosilicate clay minerals. *Journal of Hydrology*, *515*, 1–9. https://doi.org/10.1016/j.jhydrol.2014.04.029

Ohte, N., Sebestyen, S. D., Shaley, J. B., Doctor, D. H., Kendall, C., Wankel, S. D., & Boyer, E. W. (2004). Tracing sources of nitrate in snowmelt runoff using a high-resolution isotopic technique: Tracing sources of nitrate in snowmelt runoff. *Geophysical Research Letters*, *31*(21). https://doi.org/10.1029/2004GL020908

Peterson, B. J., Wollheim, W. M., Mulholland, P. J., Webster, J. R., Meyer, J. L., Tank, J. L., et al. (2001). Control of nitrogen export from watersheds by headwater streams. *Science*, *292*(5514), 86–90. https://doi.org/10.1126/science.1056874

Petrone, K., Buffam, I., & Laudon, H. (2007). Hydrologic and biotic control of nitrogen export during snowmelt: A combined conservative and reactive tracer approach. *Water Resources Research*, *43*(6), 2006WR005286. https://doi.org/10.1029/2006WR005286

Phillips, R. P., Brzostek, E., & Midgley, M. G. (2013). The mycorrhizal-associated nutrient economy: A new framework for predicting carbon–nutrient couplings in temperate forests. *New Phytologist*, *199*(1), 41–51. https://doi.org/10.1111/nph.12221

Pinay, G., Bernal, S., Abbott, B. W., Lupon, A., Marti, E., Sabater, F., & Krause, S. (2018). Riparian corridors: A new conceptual framework for assessing nitrogen buffering across biomes. *Frontiers in Environmental Science*, *6*, 47. https://doi.org/10.3389/fenvs.2018.00047

Pinay, G., Peiffer, S., De Dreuzy, J.-R., Krause, S., Hannah, D. M., Fleckenstein, J. H., et al. (2015). Upscaling nitrogen removal capacity from local hotspots to low stream orders' drainage basins. *Ecosystems*, *18*(6), 1101–1120. https://doi.org/10.1007/s10021-015-9878-5

Raymond, P. A., Saiers, J. E., & Sobczak, W. V. (2016). Hydrological and biogeochemical controls on watershed dissolved organic matter transport: Pulse-shunt concept. *Ecology*, *97*(1), 5–16. https://doi.org/10.1890/14-1684.1

Robertson, E. K., Bartoli, M., Brüchert, V., Dalsgaard, T., Hall, P. O. J., Hellemann, D., et al. (2019). Application of the isotope pairing technique in sediments: Use, challenges, and new directions. *Limnology and Oceanography: Methods*, *17*(2), 112–136. https://doi.org/10.1002/lom3.10303

Rogers, D. B., Newcomer, M. E., Raberg, J. H., Dwivedi, D., Steefel, C., Bouskill, N., et al. (2021). Modeling the impact of riparian hollows on river corridor nitrogen exports. *Frontiers in Water*, *3*, 590314. https://doi.org/10.3389/frwa.2021.590314

Rose, L. A., Elliott, E. M., & Adams, M. B. (2015). Triple nitrate isotopes indicate differing nitrate source contributions to streams across a nitrogen saturation gradient. *Ecosystems*, *18*(7), 1209–1223. https://doi.org/10.1007/s10021-015-9891-8

Ruddell, B. L., & Kumar, P. (2009). Ecohydrologic process networks: 2. Analysis and characterization: Ecohydrologic process networks, 2. *Water Resources Research*, *45*(3). https://doi.org/10.1029/2008WR007280

Schiff, S. L., Devito, K. J., Elgood, R. J., McCrindle, P. M., Spoelstra, J., & Dillon, P. (2002). Two adjacent forested catchments: Dramatically different NO_3^- export. *Water Resources Research*, *38*(12). https://doi.org/10.1029/2000WR000170

Schimel, D. S., Braswell, B. H., & Parton, W. J. (1997). Equilibration of the terrestrial water, nitrogen, and carbon cycles. *Proceedings of the National Academy of Sciences*, *94*(16), 8280–8283. https://doi.org/10.1073/pnas.94.16.8280

Sebestyen, S. D., Ross, D. S., Shanley, J. B., Elliott, E. M., Kendall, C., Campbell, J. L., et al. (2019). Unprocessed atmospheric nitrate in waters of the northern forest region in the U.S. And Canada. *Environmental Science and Technology*, *53*(7), 3620–3633. https://doi.org/10.1021/acs.est.9b01276

Sebestyen, S. D., Shanley, J. B., Boyer, E. W., Kendall, C., & Doctor, D. H. (2014). Coupled hydrological and biogeochemical processes controlling variability of nitrogen species in streamflow during autumn in an upland forest: Stream N dynamics during autumn. *Water Resources Research*, *50*(2), 1569–1591. https://doi.org/10.1002/2013WR013670

Sickman, J. O., Leydecker, A., Chang, C. C. Y., Kendall, C., Melack, J. M., Lucero, D. M., & Schimel, J. (2003). Mechanisms underlying export of N from high-elevation catchments during seasonal transitions. *Biogeochemistry*, *64*(1–3), 1–24. https://doi.org/10.1023/a:1024928317057

Sigman, D. M., Casciotti, K. L., Andreani, M., Barford, C., Galanter, M., & Böhlke, J. K. (2001). A bacterial method for the nitrogen isotopic analysis of nitrate in seawater and freshwater. *Analytical Chemistry*, *73*(17), 4145–4153. https://doi.org/10.1021/ac010088e

Siirila-Woodburn, E. R., Rhoades, A. M., Hatchett, B. J., Huning, L. S., Szinai, J., Tague, C., et al. (2021). A low-to-no snow future and its impacts on water resources in the western United States. *Nature Reviews Earth and Environment*, *2*(11), 800–819. https://doi.org/10.1038/s43017-021-00219-y

Sorensen, P. O., Beller, H. R., Bill, M., Bouskill, N. J., Hubbard, S. S., Karaoz, U., et al. (2020). The snowmelt niche differentiates three microbial life strategies that influence soil nitrogen availability during and after winter. *Frontiers in Microbiology*, *11*, 871. https://doi.org/10.3389/fmicb.2020.00871

Sprenger, M., Carroll, R. W. H., Dennedy-Frank, J., Siirila-Woodburn, E. R., Newcomer, M. E., Brown, W., et al. (2022). Variability of snow and rainfall partitioning into evapotranspiration and summer runoff across nine mountainous catchments. *Geophysical Research Letters*, *49*(13). https://doi.org/10.1029/2022GL099324

Steffen, W., Richardson, K., Rockström, J., Cornell, S. E., Fetzer, I., Bennett, E. M., et al. (2015). Planetary boundaries: Guiding human development on a changing planet. *Science*, *347*(6223), 1259855. https://doi.org/10.1126/science.1259855

Svensson, T., Lovett, G. M., & Likens, G. E. (2012). Is chloride a conservative ion in forest ecosystems? *Biogeochemistry*, *107*(1–3), 125–134. https://doi.org/10.1007/s10533-010-9538-y

Thébault, A., Clément, J.-C., Ibanez, S., Roy, J., Geremia, R. A., Pérez, C. A., et al. (2014). Nitrogen limitation and microbial diversity at the treeline. *Oikos*, *123*(6), 729–740. https://doi.org/10.1111/j.1600-0706.2013.00860.x

Thompson, S. E., Basu, N. B., Lascurain, J., Aubeneau, A., & Rao, P. S. C. (2011). Relative dominance of hydrologic versus biogeochemical factors on solute export across impact gradients: Hydrology controls solute export. *Water Resources Research*, *47*(10). https://doi.org/10.1029/2010WR009605

Tokunaga, T. K., Tran, A. P., Wan, J., Dong, W., Newman, A. W., Beutler, C. A., et al. (2022). Quantifying subsurface flow and solute transport in a snowmelt-recharged hillslope with multiyear water balance. *Water Resources Research*, *58*(12), e2022WR032902. https://doi.org/10.1029/2022WR032902

Uhlemann, S., Dafflon, B., Wainwright, H. M., Williams, K. H., Minsley, B., Zamudio, K., et al. (2022). Surface parameters and bedrock properties covary across a mountainous watershed: Insights from machine learning and geophysics. *Science Advances*, *8*(12), eabj2479. https://doi.org/10.1126/sciadv.abj2479

Wainwright, H. M., Uhlemann, S., Franklin, M., Falco, N., Bouskill, N. J., Newcomer, M. E., et al. (2022). Watershed zonation through hillslope clustering for tractably quantifying above- and below-ground watershed heterogeneity and functions. *Hydrology and Earth System Sciences*, *26*(2), 429–444. https://doi.org/10.5194/hess-26-429-2022

Wan, J., Tokunaga, T. K., Brown, W., Newman, A. W., Dong, W., Bill, M., et al. (2020). Bedrock weathering contributes to subsurface reactive nitrogen and nitrous oxide emissions. *Nature Geoscience*, *14*(14), 217–224. https://doi.org/10.1038/s41561-021-00717-0

Wan, J., Tokunaga, T. K., Brown, W., Newman, A. W., Dong, W., Bill, M., et al. (2021). Bedrock weathering contributes to subsurface reactive nitrogen and nitrous oxide emissions. *Nature Geoscience*, *14*(4), 217–224. https://doi.org/10.1038/s41561-021-00717-0

Wan, J., Tokunaga, T. K., Williams, K. H., Dong, W., Brown, W., Henderson, A. N., et al. (2019). Predicting sedimentary bedrock subsurface weathering fronts and weathering rates. *Scientific Reports*, *9*(1), 17198. https://doi.org/10.1038/s41598-019-53205-2

Wang, S., Pi, Y., Song, Y., Jiang, Y., Zhou, L., Liu, W., & Zhu, G. (2020). Hotspot of dissimilatory nitrate reduction to ammonium (DNRA) process in freshwater sediments of riparian zones. *Water Research*, *173*, 115539. https://doi.org/10.1016/j.watres.2020.115539

Ward, E. B., Duguid, M. C., Kuebbing, S. E., Lendemer, J. C., & Bradford, M. A. (2022). The functional role of ericoid mycorrhizal plants and fungi on carbon and nitrogen dynamics in forests. *18*.

Wexler, S. K., Goodale, C. L., McGuire, K. J., Bailey, S. W., & Groffman, P. M. (2014). Isotopic signals of summer denitrification in a northern hardwood forested catchment. *Proceedings of the National Academy of Sciences*, *111*(46), 16413–16418. https://doi.org/10.1073/pnas.1404321111

Winnick, M. J., Carroll, R. W. H., Williams, K. H., Maxwell, R. M., Dong, W., & Maher, K. (2017). Snowmelt controls on concentration-discharge relationships and the balance of oxidative and acid-base weathering fluxes in an alpine catchment, East River, Colorado: Acid-base versus oxidative weathering fluxes. *Water Resources Research*, *53*(3), 2507–2523. https://doi.org/10.1002/2016WR019724

Yuan, K., Zhu, Q., Li, F., Riley, W. J., Torn, M., Chu, H., et al. (2022). Causality guided machine learning model on wetland CH4 emissions across global wetlands. *Agricultural and Forest Meteorology*, *324*, 109115. https://doi.org/10.1016/j.agrformet.2022.109115

Zhi, W., & Li, L. (2020). The shallow and deep hypothesis: Subsurface vertical chemical contrasts shape nitrate export patterns from different land uses. *Environmental Science & Technology, acs.est*, *54*(19), 0c01340–11928. https://doi.org/10.1021/acs.est.0c01340

Zhi, W., Li, L., Dong, W., Brown, W., Kaye, J., Steefel, C., & Williams, K. H. (2019). Distinct source water chemistry shapes contrasting concentration-discharge patterns. *Water Resources Research*, *55*(5), 2018WR024257. https://doi.org/10.1029/2018WR024257

Zhi, W., Williams, K. H., Carroll, R. W. H., Brown, W., Dong, W., Kerins, D., & Li, L. (2020). Significant stream chemistry response to temperature variations in a high-elevation mountain watershed. *Communications Earth & Environment*, *1*(1), 43. https://doi.org/10.1038/s43247-020-00039-w

Zhu, Q., Castellano, M. J., & Yang, G. (2018). Coupling soil water processes and the nitrogen cycle across spatial scales: Potentials, bottlenecks and solutions. *Earth-Science Reviews*, *187*, 248–258. https://doi.org/10.1016/j.earscirev.2018.10.005

Zogg, G. P., Zak, D. R., Pregitzer, K. S., & Burton, A. J. (2000). Microbial immobilization and the retention of anthropogenic nitrate in a Northern hardwood forest. *Ecology*, *81*(7), 1858–1866. https://doi.org/10.1890/0012-9658(2000)081[1858:MIATRO]2.0.CO;2

References From the Supporting Information

Buchwald, C., & Casciotti, K. L. (2010). Oxygen isotopic fractionation and exchange during bacterial nitrite oxidation. *Limnology & Oceanography*, *55*(3), 1064–1074. https://doi.org/10.4319/lo.2010.55.3.1064

Casciotti, K. L., McIlvin, M., & Buchwald, C. (2010). Oxygen isotopic exchange and fractionation during bacterial ammonia oxidation. *Limnology & Oceanography*, *55*(2), 753–762. https://doi.org/10.4319/lo.2010.55.2.0753

Casciotti, K. L., Sigman, D. M., Hastings, M. G., Böhlke, J. K., & Hilkert, A. (2002). Measurement of the oxygen isotopic composition of nitrate in seawater and freshwater using the denitrifier method. *Analytical Chemistry*, *74*(19), 4905–4912. https://doi.org/10.1021/ac020113w

Fang, Y., Koba, K., Makabe, A., Zhu, F., Fan, S., Liu, X., & Yoh, M. (2012). Low δ^{18}O values of nitrate produced from nitrification in temperate forest soils. *Environmental Science and Technology*, *46*(16), 8723–8730. https://doi.org/10.1021/es300510r

Kendall, C., Campbell, D. H., Burns, D. A., Shanley, J. B., Silva, S. R., & Chang, C. C. Y. (1995). Tracing sources of nitrate in snowmelt runoff using the oxygen and nitrogen isotopic compositions of nitrate, *9*.